NTNU

Norwegian University of
Science and Technology

Investigation of Cogging Torque of a Downhole Drilling Machine and Optimization of Electrical Machine

Aasim Ullah

Investigation of Cogging Torque of Downhole Drilling Machine and Optimization of Electrical Machine

Aasim Ullah, Department of Electrical Power, Norwegian University of Science & Technology,
(NTNU), Trondheim, Norway. aasim@stud.ntnu.no

Abstract:

This paper is a report on master thesis project conducted in cooperation with SMARTMOTOR AS and NTNU. The research for electrical downhole drilling machine has developed for decades. Permanent Magnet is a new addition in this arena. SMARTMOTOR AS built a downhole drilling machine which is needed to compare with machines from other competitors of the market. This machine has 10% cogging torque over its rated torque. The reason of this cogging torque and possible solutions has been investigated throughout this project. And a new geometry and design of the rotor (with 10 poles) is suggested for the machine in this report. Measurement shows the newer design is less sensitivity to eccentricity. at nominal load and speed. Lastly, flux weakening and magnet working point of the machine also investigated.

In this report it is concluded that out of 3 experimental designs, the design with less epoxy and more magnet offer better performance regarding voltage waveform and vibrations. It is superior in terms of torque per weight. The other designs however allow easier manufacturing, better efficiency and shorter length of machine. It It is therefore concluded that the last design with less epoxy can be a suitable alternative rotor design for the built up machine which can reduce the existing cogging torque upto 83.4%.

The end part of the paper describes a template-style of a generic electromagnetic modeling tool for the analysis and optimization of Electrical Machines. Further accurate virtual prototypes can then be produced to help designers provide answers on the performance of specific machine designs rapidly. And further investigations to identify the design characteristics of the perfect machine.

A two and three-dimensional FEA model for a generator and motor can be created in minutes, investigations to identify the design characteristics of the perfect machine. Optimization tool assists designers to find the 'best' solution automatically. The tool is structured to allow creation and analysis of customized geometries, including special proprietary features. A new Matlab-based script is developed in order to handle the optimization process of electrical machine which will be used in the finite element analysis. The script saves the designer's valuable time.

It is concluded that 'fmincon-constrained nonlinear minimization' method in new optimization tool of MATLAB is more accurate and less time consuming compared to the method for optimization.

The report explains a modern design procedure which uses both analytical and numerical analysis. The numerical analysis uses finite element analysis that is performed in Comsol mostly.

Index Terms— Cogging Torque, permanent magnet, state of art, skew effect, flux weakening, magnet working point.

I. INTRODUCTION

In last few years drilling machine technology has intensively been developed and it is one of the fastest growing technologies. In recent year this research field of arena has grown in a bigger extent. General comparison of different machines is difficult. It depends on which parameter is chosen for comparison. As down-hole-motor drilling motor might be developed to work with a broad range of available basic down hole drilling equipment, along with identification of opportunities for technology. Considering market potential a brief investigation of comparison has been done in this report.

In near future electrical downhole machine will be an important element for improved utilization of existing wells. In Fig 1, the built up machine by SMARTMOTOR AS is shown before no load test. And the real rotor with hallbach array design is set inside it. The machine has been tested with dummy rotor first.

Figure 1: The rotor is fitted inside the stator of drilling machine

II. PROJECT TASK AND OBJECTIVE

The existing drilling machine is compared in terms of Key Performance Indicator (KPI). In this part the stated task is to identify potential products with state of the art and scaling of Badger machine. Later the cogging torque of badger machine made by Smartmotor AS has been investigated. The project task covers the following pointers:

1. To investigate how much cogging torque the machine has
2. To investigate the reason of cogging torque
3. To investigate if the rotor is non-concentric/ non-aligned
4. To investigate sensitivity of alignment and non-concentricity.
5. To make 2D FEM model and investigate non-concentric in that one.
6. To investigate various designs besides the proposed 10 pole design. And to suggest alternative design that are more robust. For Analytical/numerical Analysis:
  - FEM analysis for case of interest.
  - Parametric model- Geometry/Parameter are variable.
7. To design a machine which is less sensitive to eccentric or bad assembly that can tolerate some eccentricity or uneven mounting of magnets.
8. To optimize the design to fullfill :
 - performance requirement, Torque, Efficiency
 - least cogging sensitivity to eccentricity.
9. To investigate lower nominal torque at same current.
10. To build a new rotor for promising new design and test it.

Objective:

According to the project task, the author is going to investigate a specification given by a customer. A new design of rotor is developed by the author in order to take account the company-specific features and new ideas that are introduced in this case.

The author is supposed to find an optimization procedure for electrical machine in a quantitative comparison. The author then must demonstrate methods and tools to be used in such a modern design and in general illustrate how classical challenges such as losses, vibrations, air gap length and cogging torques are taken into account.

In addition the author shall focus on the investigation of the buillt up machine for downhole drilling applications.

III. STATE OF THE ART

In this study the author is going to design a state-of-the-art for the built up downhole drilling machine. In cooperation with an industrial company, SmartMotor AS, a machine for downhole drilling application is to be designed to fulfill a given set of general specifications. In introduction (Part I) it is mentioned earlier it's hard to fairly compare a number of machines as there are parameters to consider. The way to compare them is called 'State of Art'.

The terms that can be considered for comparison are: efficiency (%), tangential tension (kN/m^2), length of machine (m), torque density (Nm/kg), power density (W/kg) etc. Here the best outputs of different comparison in P-Kg VS T-Kg curve have been chosen. In the plot the curve gives the information to the buyers how compact one machine is comparing the machines with other companies.

This is a considered a good way of comparison. Only considering torque or speed is nonetheless a good idea of comparison. In that case a machine with higher torque and speed can defeat a machine with lower torque and speed which has better efficiency in comparison.

A. Identify state of art

Hydraulic machine is more usual than electrical machine for drilling purpose. Permanent magnet machine for drilling is a new technology. Machine performance from different companies has been figured out by the author and the data has been investigated in this section. The companies that have machines of good performances in drilling are:
 1. Rugao Yaou Co Ltd, China
 2. Wenzel Downhole tool Ltd, Calgary, Alberta, Canada.
 3. Torquato Drilling Accessories, USA
 4. NOV (National Oilwell Varco),USA
 5. Torquato Drilling Accessories, USA

The down-hole drilling machine built by SMARTMOTOR AS is of 127 mm (5 inch) Outer Diameter. The built machine of 5inch OD is now to be compared with the existing machines available in market from other competitors. The state of the art in Fig1 shows some plotting of good machines from 3 different companies- Servostar, Moog and Leroy Somer (LSRPM).
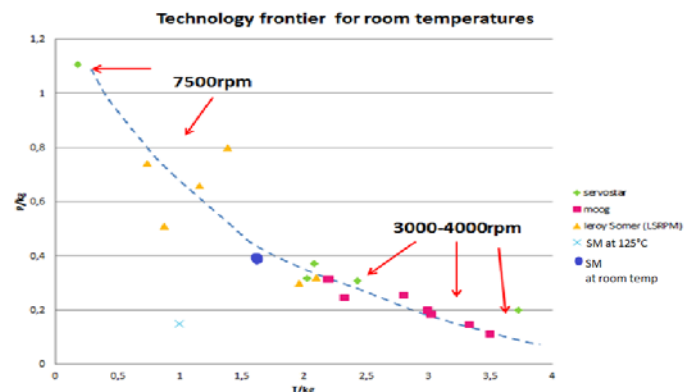

Figure 2: Technology frontier for room temperature.

Two factors of KPI (Key Power Factor) are power density and torque density. And in Fig 2 the state-of-the-art performance of mentioned KPIs has been investigated and visualized them in graph. Out of hundred machines only the machine of best performance is selected from company catalogues for this investigation. In Fig2, the position of Smartmotor machine at ambient temperature (125℃) is lower than the state of art –belt, as it has built for higher temperature.

The same machine is investigated with SMARTTOOL [1] data with room temperature and plotted in the same figure. The new machine has closer position to the belt. Though, this new machine position is a theoretical placement only. As it is not tested for room temperature yet.

The higher speed and lower speed machines has been plotted in the figures in order to find out the state of art belt. For drilling machine research it is therefore suggested to investigate the same graph in terms of volume rather than kg. As the volume of machine is a matter of concern in drilling purpose. Detailed Company data is enclosed in Appendix A with both weights and volumes data of machine.

B. Scaling Badger Machine

The down-hole drilling machine built by SMARTMOTOR AS is of 127 mm (5 inch) Outer Diameter. The other sizes (73mm, 89mm, 95mm OD) those are available in market also has been investigated by the author. In the report it is compared in terms of output machine design parameters and characteristic parameters like air gap, stator inner diameter, efficiency, Pf & current loading etc for smaller scale machine with existing badger prototype machine (5 inches Outer Diameter) by using SMARTTOOL.[1]

IV.   INVESTIGATING COGGING TORQUE

Cogging torque of electrical motors is the torque due to the interaction between the permanent magnets of the rotor and the stator slots of a Permanent Magnet (PM) machine. It is also known as detent or 'no-current' torque. Cogging torque is an undesirable component for the operation of such a motor. It is especially prominent at lower speeds, with the symptom of jerkiness. [2]

A. Cogging Torque minimization techniques

Cogging torque minimization is necessary for low torque ripple applications such as precision tooling etc. Various techniques are available but few techniques are proved to be effective in mass production under manufacturing tolerances/variations. The research provides a design approach to minimize cogging torque by making the motor robust to manufacturing variations and dimensional tolerances. Several control and noise factors are identified to apply the robust design technique. The quality of robustness is judged by the signal-to-noise ratio. A trade-off is exercised to maximize output torque in selecting the control parameters. The research shows the effectiveness of such design techniques in designing motors for mass production without adding cost or complexity. Experimentation by modeling has been chosen using finite element analysis. Motors using the optimized parameters are built and tested thus verifying the design approach. [3]

In general, cogging torque minimization in usual machines can be accomplished in two manners: Modifications from the stator side and rotor side. Classification of these techniques can be shown in Fig. 3. An important drawback of modifying the stator to minimize the cogging torque component is that it complicates the stator manufacturing and consequently increases the manufacturing cost of the machine. Therefore, modifications from the stator side are not practical in downhole drilling machines usually not preferred.
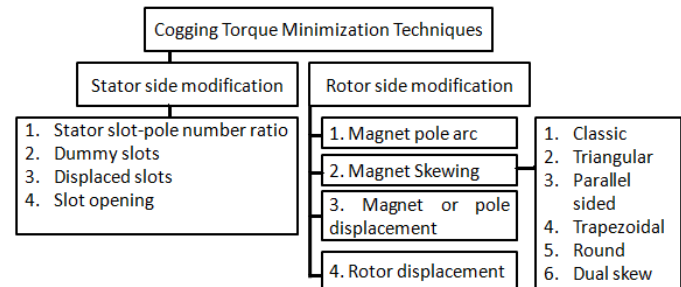

Figure 3: Cogging Torque minimization techniques

In Fig. 3 different cogging torque minimization techniques are shown.

B. Physical observation

The machine built by Smartmotor AS has been investigated and a 2Nm Cogging torque has been measured. Whereas the rated torque of the machine is 20Nm. It means the machine has 10% cogging torque to its rated torque. A few points can be mentioned after physical observation of the machine.

- There are arbitrary misplacement of magnets.
- 0.5-0.8mm physical depth variation in magnet.
- The worst case is 0-0.08mm eccentric from centre.
- Mechanical tolerance   is a point of consideration for investigating cogging torque.
- Impact for harmonics can also be considered.

V.   NEW DESIGN WITH 10 MAGNETS

In this part a new design of rotor has been designed with 10 magnets and epoxy as shown in Fig. 4b The author is grateful to Astrid Røkke for her help in this part.

The design is built up in three different stages. In first existing design Hallbach array is used with forty magnets. In this design the rotating pattern of permanent magnets for hallbach array can be continued indefinitely. The effect of this arrangement is roughly similar to many horseshoe magnets adjacent to each other, with similar pole touching. In Fig 4a the first design is drawn with hallbach array. While in the new design the magnet orientation is done radial outward and radial inward alternatively for 10 magnets.

Magnet orientation for different directions using Fig 2 is included in Table 1. These directions were used in the magnets of Hallbach Array design (Fig 4a). According to Fig 5, first design is investigated with hallbach array and later with three different magnet and epoxy sizes.
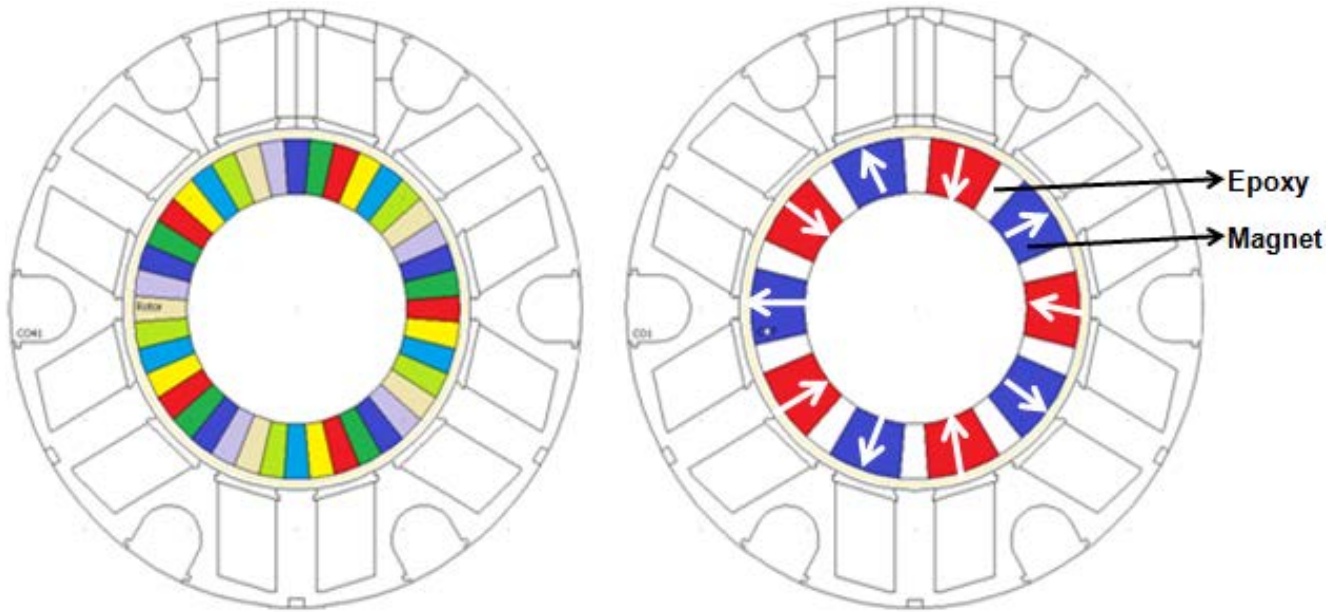
Figure 4: Different magnet arrangements: (a)Hallbach array (b) conventional N-S array
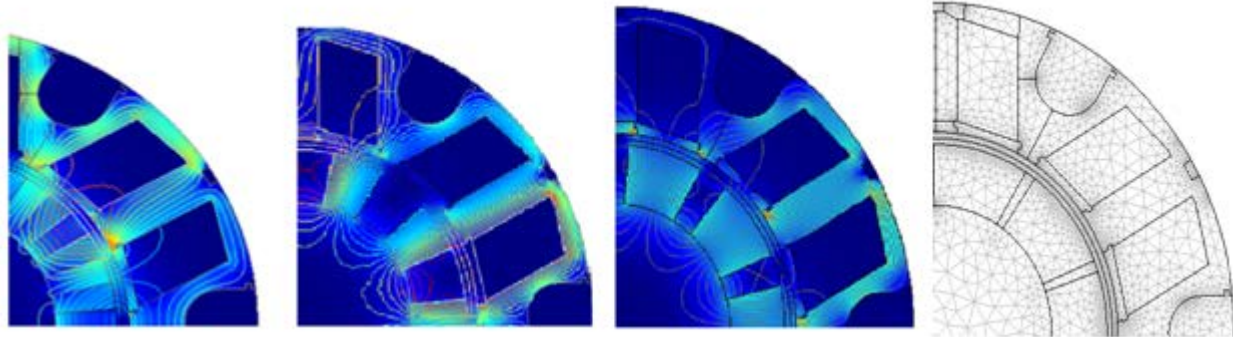

Figure 5: New design of rotor : (a) with hallbach array (b)Magnet-Epoxy (50%-50%) (c)Magnet-Epoxy (75%-25%) (d) Magnet-Epoxy (90%-10%)

While in the new design with ten magnets the orientation was alternatively Samarium Cobult radial inward and outward like table 2.
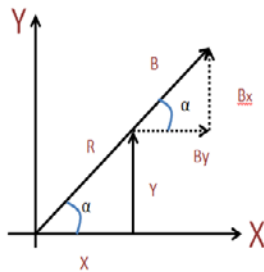
W	Br/sqrt(2)*(x/R-y/R)	Br/sqrt(2)*(x/R+y/R)
NW	Br/R*x	Br/R*y
N	Br/sqrt(2)*(x/R+y/R)	Br/sqrt(2)*(-x/R+y/R)
NE	Br*y/R	-Br*x/R

Table 1: Magnet Direction of Hallbach Array used in previous rotor

New design with 10 magnet (filled with epoxy in between) have half magnet size.

Direction	X-axis	Y-axis
N	Br[T]*x/sqrt(x^2+y^2)	Br[T]*y/sqrt(x^2+y^2)
S	-Br[T]*x/sqrt(x^2+y^2)	-Br[T]*y/sqrt(x^2+y^2)

Table 2: Magnet Direction used in 10 magnets machine

Figure 2: Magnet orientation in Hallbach Array design

Direction	X-axis	Y-axis
N	Br/sqrt(2)*(x/R+y/R)	Br/sqrt(2)*(-x/R+y/R)
NE	Br*y/R	-Br*x/R
E	Br/sqrt(2)*(-x/R+y/R)	Br/sqrt(2)*(-x/R-y/R)
SE	-Br/R*x	-Br/R*y
S	Br/sqrt(2)*(-x/R-y/R)	Br/sqrt(2)*(x/R-y/R)
SW	-Br*y/R	Br*x/R

A. THD

The comparison of Back Emf and THD (Third Harmonic Distortion) from two different designs is mentioned in Table 3. And in the new design the values are much reduced which is also a significant improvement.

	Design with Hallbach Array		Design with 10 magnets (Magnet-Epoxy (90%-10%))	
Emf	Voltage	THD	Voltage	THD
1	16,4397	5,339%	8,0057	3,4845%
2	16,4397	4,7177%	8,0057	4,0139%
3	16,4395	4,5481%	8,0057	4,1605%

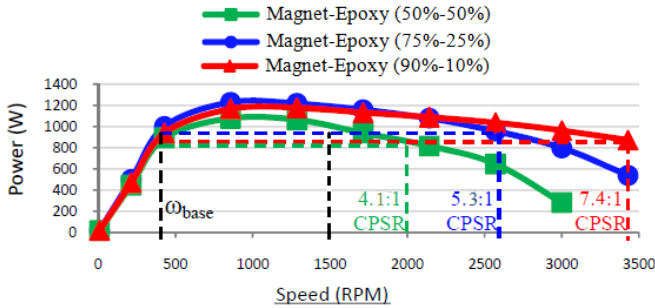Table 3 : Back Emf and Third Harmonic Distortion of two different design

B. CPSR

Figure 6: Speed VS power performance for various power design

Fig.6 compares the power versus speed characteristics of the three models. It can be seen that the machine with more epoxy has the weakest performance amongst the three designs It produces the lowest torque and power magnitudes at all speeds and the poorest field weakening performance. Although the machine with less epoxy produces the highest torque and power density up to 2100rpm, the machine with less epoxy demonstrated better fieldweakening performance with a CPSR (Constant Power Speed Range) up to 7:4.

C. Problem with 3 designs

With 50%magnet-50% epoxy the machine grows longer, which is a big concern for downhole drilling application. The machine is at its best with the machine with 75%magnet-25% epoxy. Still the length of the machine is not close to compromise enough. So the next design the rotor with 90% magnet-10% epoxy investigated.

As the machine with 90% magnet happens to be a good design. Other techniques of minimizing torque has been investigated for this design in later part of this report.

VI. ALTERNATIVE MAGNET SKEWING

Skewing, is a good method of reducing cogging torque. Skewing on the contrary to fractional slot windings, is trying to zero $dR/d\theta$ over each pole pitch either by skewing the magnets or the slots. Though both skewing techniques have disadvantage. Skewing the slots increase the ohmic losses due to longer slots, while skewing the magnets increase the magnet cost. Another important disadvantage with skewing is the formation of normal force. [4]

The cogging torque in the machine can be expressed as T (θ) = dW (θ) / d$\phi(\theta)$ where W is the magnetic energy in the machine, and ϕ is the angular position of the rotor. The calculation of these forces requires detailed modeling of the machine. The number of cogging periods per electrical period is however easy to find. Cogging Torque can be reduced by skewing stator stack or magnet pole.

Skewing the stator stack is to spatially skew one end of the stator stack a few degrees with respect to the other end of the stack. A full skew of one slot pitch can also be implemented to reduce the cogging torque. One slot pitch is an arc covering one slot.

The magnet pole shaping, linear skew of rotor magnets or stator, step-skew of the magnets, dummy slots in stator teeth, shifting of magnets, etc. are well known techniques for reducing the cogging torque. Bianchi et al. [5] reported a unified approach in analyzing the cogging torque minimization techniques. The research is well sup-ported through simulation and experimental results and also discussed the possible effects of these methods on back-emf. Slemon et al. [6-7] investigated the effect of pole width and tooth/slot ratio for minimizing cogging torque in PM motors. Zhu et al. [8] presented the effect of slot/pole combination on cogging torque amplitude and frequency. Favre et al. [9] have presented a comprehensive approach for reducing cogging and ripple torque. These methods are good for minimizing the cogging torque but do not address the effect of manufacturing variations and tolerances [10].
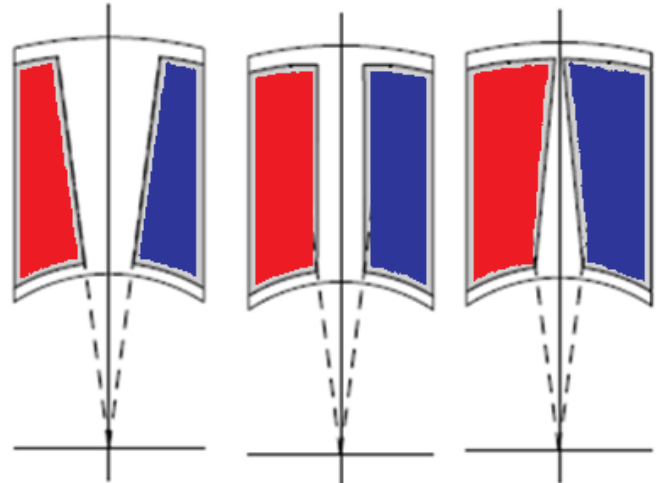

Figure 7: a) unskewed b) parallal-sided magnet c) triangular magnet skew

In Fig 7 few possible magnet skewing shapes are shown for the new design.

A. Normal Skewing

In the beginning of experiment normal skewing of magnet has been chosen. In Fig 8 skewed magnet ABCD is shown with its new position ABC'D'.
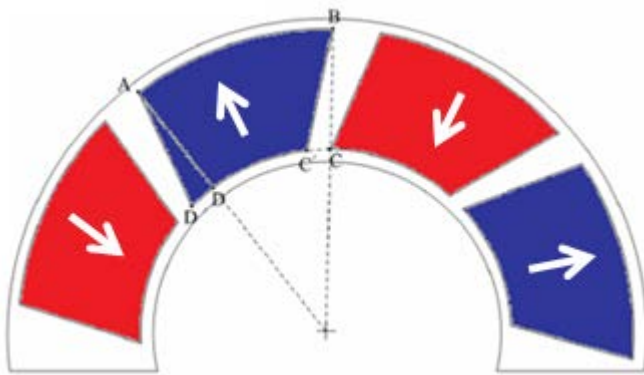
Figure 8: Magnet ABCD is skewed to ABC'D'

In Fig 8 magnet skewed with the new shape is compared with the original shape of rotor in terms of cogging torque at different rotor position. The PMs are of the general shape and at the optimized shape are shown in Fig. 9. By using FEM and the peak cogging torque decreases from 1.770 Nm to 0.816 Nm with skewing. The value of of flux/L is 0.0413 and 0.0377 respectively. The optimal shape of each PM represented by the number of flexible PM blocks is given in Table 4.
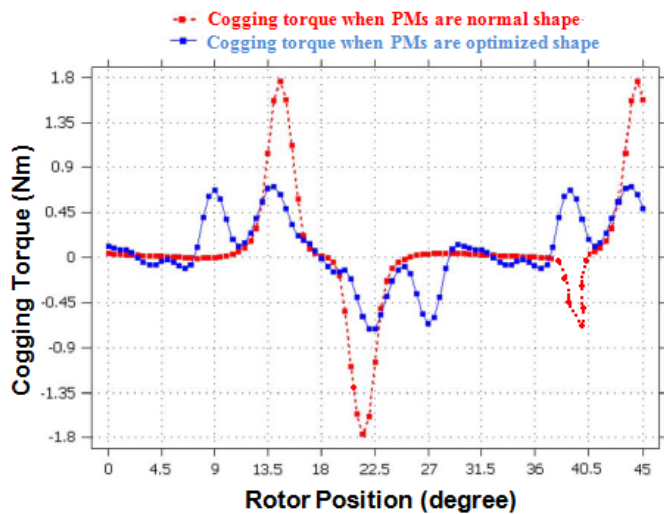
Figure 9: Cogging Torque with two different shape of magnet

	Cogging Torque (Nm)	flux/L (wb/m)
With general shape	1.770	0.0413
With optimal shape	0.816	0.0377

Table 4 : Comparison between two different shape of magnet result
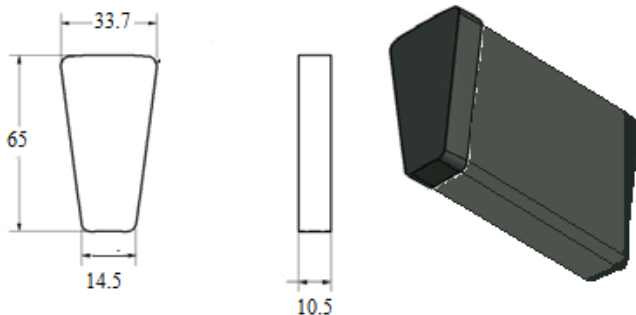
Figure 10: Magnet dimension for proposed design

In Fig 10 the chosen magnet for this design is shown with its real shape and dimension.

B. Skewing with different skew angel
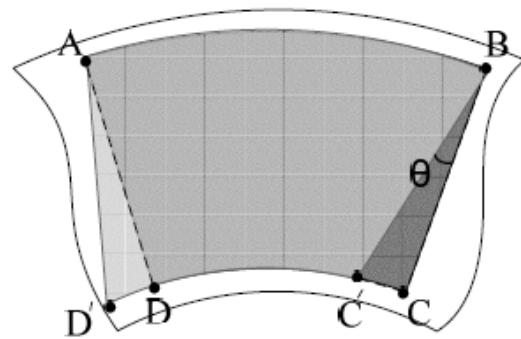
Figure 11: Magnet ABCD is skewed to ABC'D'

As displayed in Fig. 11, fan-shaped magnet ABCD is skewed to ABC'D', and the mechanical skew angle (θ) is the angle between the edges of the fan-shaped magnet and the skewed magnet on the same side.

As the θ-angle decreases, air gap flux increases in proportion to the magnet surface area. An increase of CPSR was also seen as V-angle decreased from 120° to 60°. A maximum CPSR of 10:1 was achieved for the model with a θ angle of 60°, after which the CPSR began to fall despite an increase in torque generated at 60°.
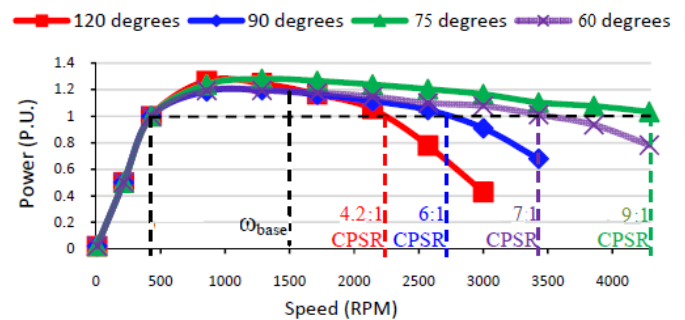

Figure 12: Speed versus power performance for various θ-angles

In Fig 12 Speed versus power performance for various θ-angles is shown.
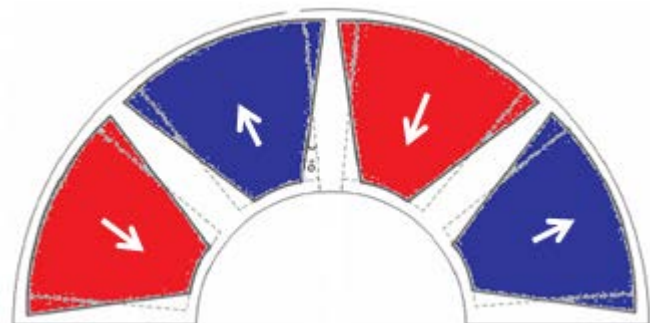
C. Triangal Skewing

Figure 13: Triangular skewing

For the machine skewing may be introduced by bringing the sides of the magnets at the rotor OD closer together while they are moved farther apart at the rotor ID, as shown in Fig. 13, thereby resulting in a triangular shaped airspace between adjacent magnets is implemented here. The cogging torque waveform has been determined for four different skew angles, with the magnet surface area maintained constant. As can be seen from Fig. 15, a significant reduction in the cogging torque can be achieved as the skew angle, δ, is increased, an 80.3% reduction in the peak cogging torque being achieved when δ = 20.5 mech.
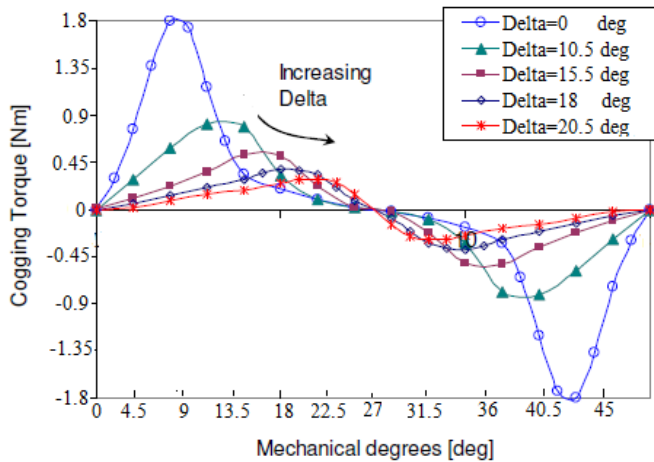
Figure 14: Cogging torque as a function of rotor angle at different skewing Angle

In Fig 14 the COMSOL ASCII values for cogging torque in transient solution has been used. The figure shows the variation of cogging torque when the magnet pole is skewed and different degrees of skewing are presented. Here Fractional pitch covers most of the full skew. The optimized cogging also presented on the same graph. The graph shows that the skewing angle plays an important role in reducing the cogging torque. The closer the skewing angle to a full skew, the smaller the resulting cogging torque.

However, skewing can add complexity to the manufacturing process, thus additional cost of the final product can be expected. Skewing the magnet requires that the magnet be shaped properly, which may add to the manufacturing cost. Skewing the stator may complicate the winding installation, reduces the effective slot area, and increases the conductor length (e.g., increases the stator resistance). [11]

D.   Slot-pitch Skewing

Fig.15 shows the variation of the cogging torque waveform of the reference machine as the skew angle is varied from a ¼ slot-pitch to 3/2 slot-pitches. Peak cogging Torque reduces with the experiment results of different slot-pitch skewing. Out of all these slot-pitch skewing 3/2 slot pitch provides a very low cogging torque which can be a good solution for the design.
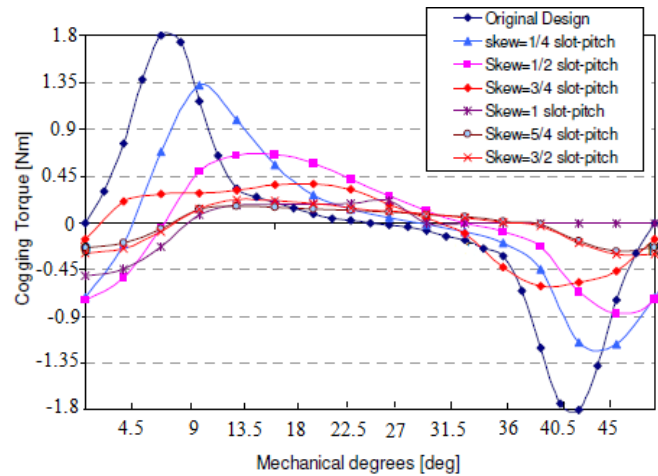

Figure 15: Cogging torque as a function of rotor angle at different skewing

VII.   COGGING TORQUE MINIMIZATION (COMSOL RESULTS)

A motor as a device converts electrical energy (input signal being the voltage or current) into mechanical energy (output signal being the torque or speed). Cogging torque is a phenomenon without any current input to the motor (a nondynamic case). Maximizing the output torque with current input to the motor (a dynamic case) may not minimize the cogging torque. Hence the problem of minimizing cogging torque lends itself to a non-dynamic case and smaller-the better (STB) response is the obvious choice for minimizing cogging torque.

For this design optimization study experimentation by finite element modeling has been chosen. The finite element modeling setup has been verified with a test motor whose noise factors specifically the magnet placement and their dimensional design parameters were measured after it was assembled. The measured values were imported into the finite element simulation model. Fig. 17 shows the comparison between the test and modeled cogging torque plots for the test motor. The results confirm the validity of choosing finite element modeling for the design of experiments. [3]
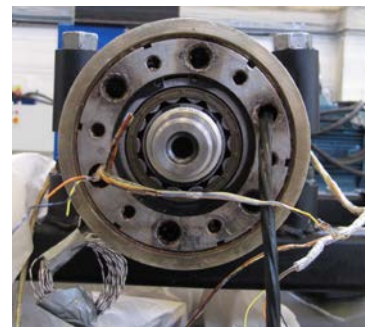

Figure 16: The machine with its full periphery to fix the temp sensor

The problem of minimizing cogging torque lends itself to a non-dynamic case and smaller-the better response is the obvious choice for minimizing cogging torque. In Fig 17 it is shown the matching of Cogging Torque in different position for model machine and COMSOL result. The result matches

in many points for both cases. In this position we can rely on the experiment data.
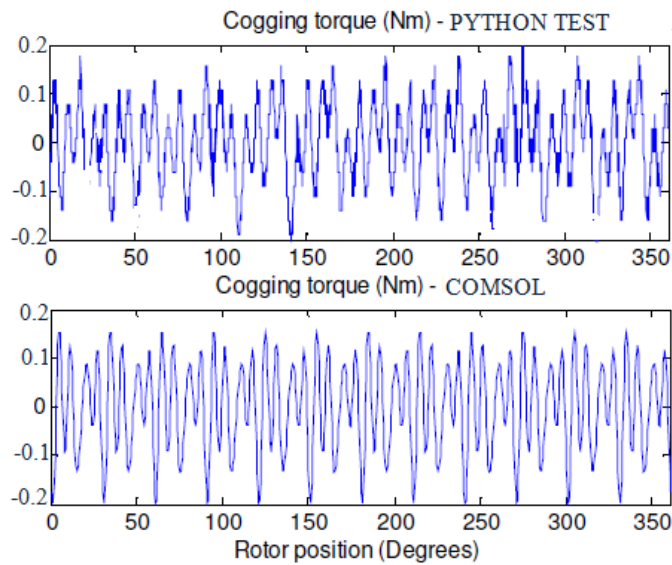

Figure 17: Correlation between modeling and test result

Fig. 17 shows the comparison between the test and modeled cogging torque plots for the test motor. The results confirm the validity of choosing finite element modeling for the design of experiments.

Figure 18: Fixing the temperature sensor

During the experiment the sensor was damaged due to overheating, which is shown fixing in Fig 16 and 18.

Measurement:

The author is grateful to Eirik Mathius Husum from Smartmotro AS for his help in this part. A rough measurement of the cogging in Badger machine has been done. The equipment used is a torque transducer, where output voltage is measured on a multimeter. No logging is done of the voltage, but the results for each position were written down by hand.

Test procedure:

A torque meter was connected to the shaft of Badger machine2 via a flexible coupling. The other end of the torque

meter was connected to a smaller shaft via a flexible coupling. Due to the flexible couplings, and the absence of bearings on the free end of the torque meter, the setup was rather wobbly, and the measurements are therefore not very reliable. The shaft was rotated slowly by hand. The cogging torque can easily be felt when rotating by hand, and it was noticed that there were 30 positions in which the rotor got stuck during one revolution.
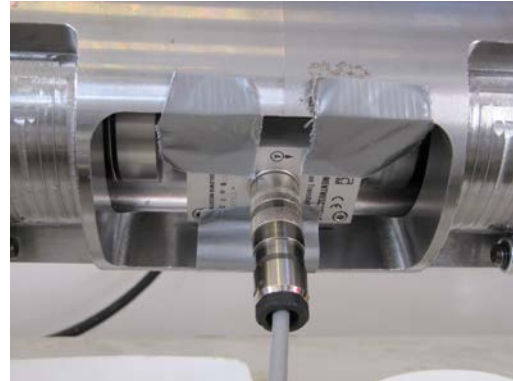

Figure 19: torquemeter to measure the torque in machine

The DC-voltage output of the torque meter was measured on a multimeter, and the approximate maximum voltage between each of the 30 positions was written. It can be noticed that in every consecutive third position the peak torque and voltage was higher than other positions. And there was a two lower torque position in between. Now, the rotor position and torque will be investigated against the direction of cogging torque. It was easy to measure the high maximum torques; as at these positions it was possible to twist the rotor against the direction of the cogging force. At lower torques, one had to be careful when doing this, if not the rotor would jump to the next position before any voltage (torque) could be read on the multimeter. It is therefore likely that some of the lower torques should have been somewhat higher. Regardless of this, one could easily feel a high torque like previous test for every third position with two lower torques in between, which is also indicated in the Fig 20.
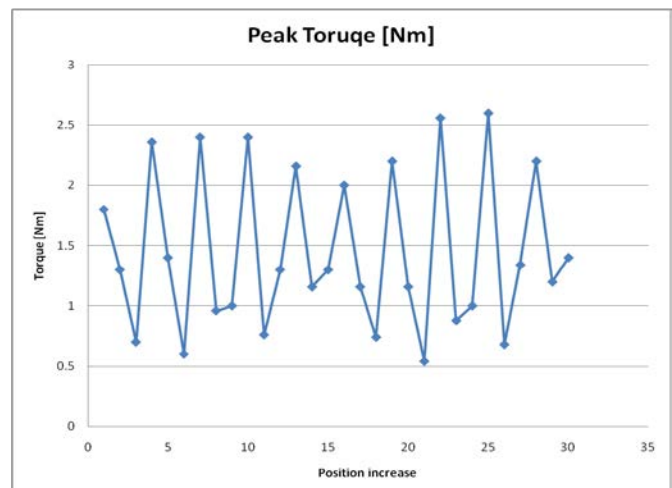

Figure 20: Approximate torque between the different rotor positions

VIII. INVESTIGATION WITH ECCENTRIC DESIGN

To investigate the performance of machine from analytical calculation are not always perfect enough. It is then need Finite Element Analysis (FEA) for further accurate result. With FEA method it is much easier to design calculations for inductance, air gap flux, magnet leakage, iron losses, back emf and cogging torque.

"COMSOL Multiphysics" is a FEA simulation software which facilitates all steps in modeling process. In COMSOL, custom definition of geometry and meshing are possible. Physics can also be specified to fit the purpose. The results can be visualized, with illustrations, graphics and numbers after the multi physical problem is solved.

A. Higher flux density:

The FEA of this project is performed by COMSOL [12]. A design with a rotor 0.08mm out of center has been drawn and investigated thereby.
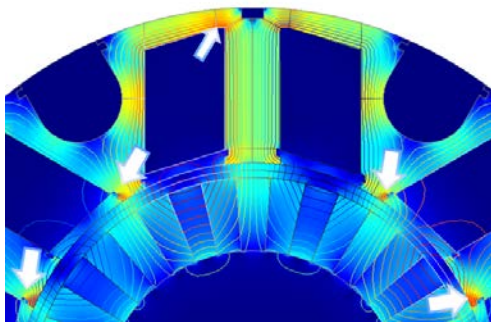
Figure 21: Higher flux densities in different position of stator-upper part
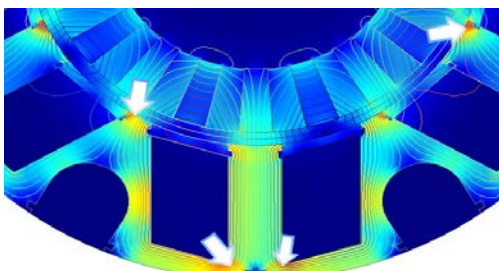
Figure 22: Higher flux densities in different position of stator-lower part

Due to eccentric position of rotor higher flux densities has been observed in various position of rotor. In Fig 21 and Fig 22 It has been indicated with arrow marks. In this position the flux densities are about 1.9-2.1T.
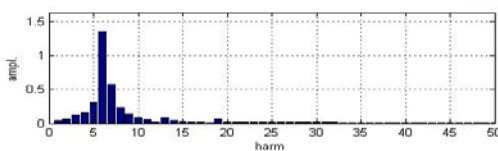
B. Harmonic distortion:

Figure 23: Cogging Torque with 6th harmonic distortion

In eccentric condition cogging torque with 6th harmonic condition also has been observed. Detail figures of COMSOL simulation are attached in Appendix B.
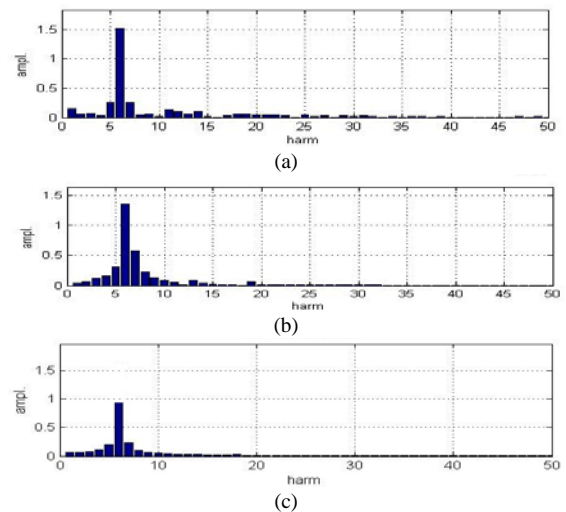

Figure 24: Cogging Torque with 6th harmonic distortion (a) normal condition(b) Eccentric condition (c) with new 10 magnet design (Magnet90%-Epoxy10%)

In Fig 24 cogging torque with 6th harmonic distortion of 10 magnets is shown in three different conditions. Whereas in the new 10 magnets design the 6th harmonic distortion reduced comparing the other two designs. Detail figures of COMSOL simulation for this new design are attached in Appendix C, D, E for Design with Magnet-Epoxy (50%-50%), Design with Magnet-Epoxy (75%-25%), Design with Magnet-Epoxy (90%-10%) respectively.

C. Winding and distribution function:

From investigation of this PM machines have a stator mmf distribution with fewer poles than in the rotor. This is illustrated in Fig. 25 for a 10 pole PMSM. The stator mmf harmonic component interacting in the mean torque production is not the fundamental, but a higher harmonic component of order equal to the number of pole pairs p/2. It is then can be called as "main harmonic" component or "synchronous frequency component". The order of the synchronous frequency component for the 10 pole machine is then 10/2= 5 (see first line under the spectra in Fig. 25). Another possible description of the winding is to define the main harmonic component as the fundamental, considering electrical angle instead of mechanical angle. The relation between the two sets of harmonic orders is shown under the spectra of Fig.25-27 for the 10 pole machine. This implies that all the harmonics of mechanical order lower than p/2 are now sub-harmonics i.e. with electrical orders of fractional values lower than 1.

Besides if all the harmonics of fractional values are taken away from the true mmf, the reduced mmf is corresponding to the mmf of the PMSM . This is illustrated for the 10-pole/12-slot PMSM in Fig. 26 and Fig 27. Therefore, when calculating the field distribution, all the harmonics should be considered in order to find a distribution. The phase resistance should be calculated

differently for the two types of windings due to the shorter end-windings of the machine. Finally, the mmf curve and harmonic component is calculated from the field distribution by taking all the harmonics into account. The main component gives the magnetizing inductance but the harmonic components contribute to the leakage inductance that is not negligible for machines [13]

In Fig 26 and 27 winding and distribution function for fractional winding distribution is portrayed respectively.

It can be shown that the sub-harmonic components in the mmf (and all other orders than kp/2, k being an integer) do not play any role in the analytical calculations of the back-emf and the mean value of the torque. It is then convenient to have the "synchronous-component" winding factor equal to the component of order 1, disregarding the harmonics of fractional orders.
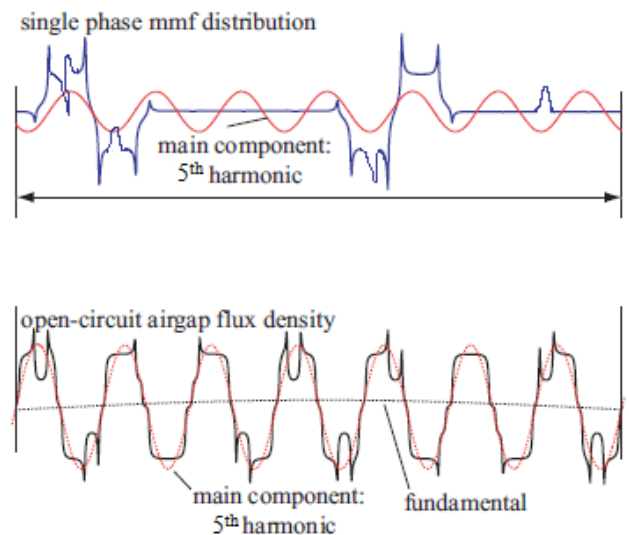
Figure 25: Mmf distribution and open-circuit airgap flux density for the 10 pole machine
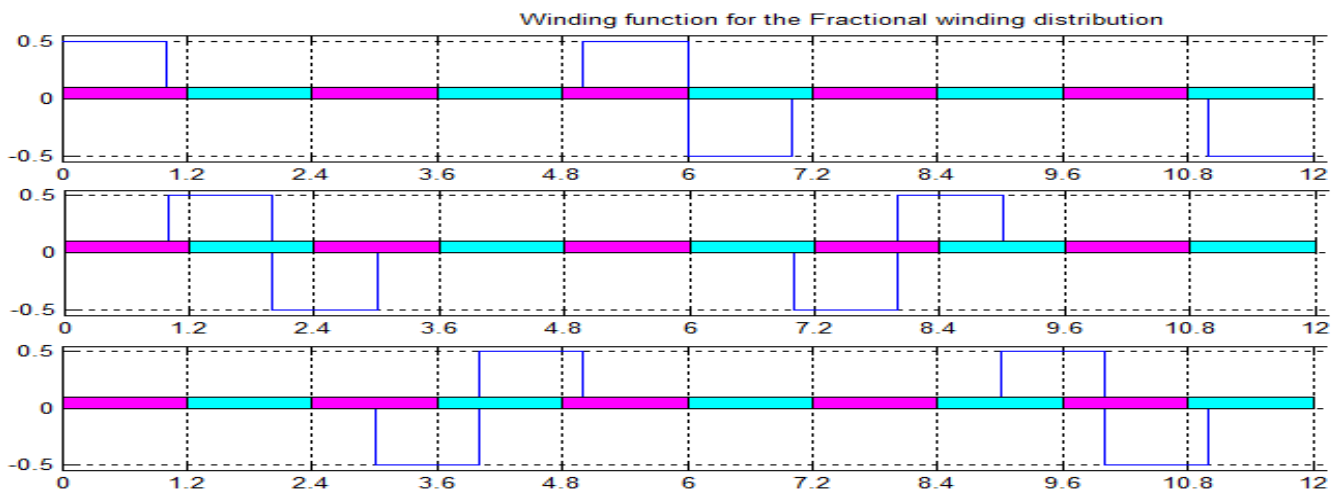
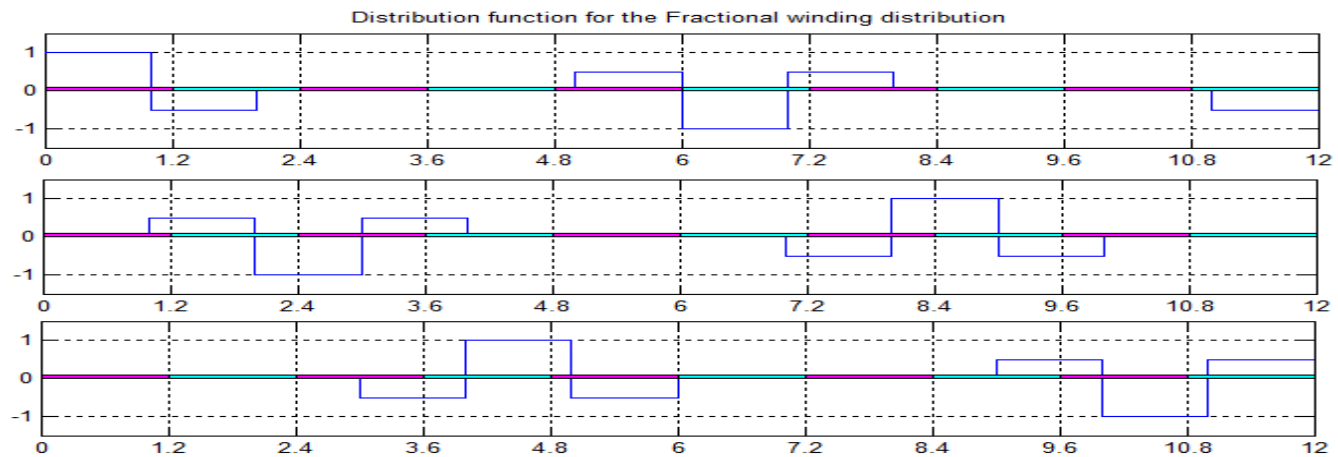Figure 26: Winding function for fractional winding distribution

Figure 27: Distribution function for fractional winding distribution

IX. NO LOAD TEST, COGGING TORQUE AND LOSES

Figure 28: Setup for no-load test

Cogging torque at different motor position has been investigated during no load test. The cogging torque, torque ripple and output torque are considered while most emphasize isgiven on the cogging torque without degrading the main output or the torque ripple performance. air gap length, magnet thickness etc are kept constant, even though they may have significant influence on cogging torque.

Figure 29:Test results at different speed

The control factors (like Airgap, Airgap OD, Rotor to stator

eccentricity, Magnet pole shape) are chosen in such way that it has minimum effect on torque output while significantly influences the cogging torque.

Fig. 29 shows the cogging torque plot for six test motors measured at 100 rpm, 200rpm,300rpm, 400rpm, 500rpm, 600rpm. The speed has controlled using Python programming in Smartmotor Lab.

Losses:

The 10 pole machine with hallbach array rotor have no load losses of 27..4W and 54 W at 400 and 800 rpm respectively. This is the same as the new 10 pole rotor at 400 rpm, but more at 800 rpm. Iron losses are frequency dependent, and increases faster at higher frequencies, and the results show how the higher fundamental frequency is more important at higher rpms. The losses are likely to have increased at 1000 rpm as well, but the coarse torque measurements at a 0.1Nm resolution and probably changed windage makes this hard to measure.

These results calculated directly from COMSOL, more time and effort are deserved to find loss of machine more accurately.

X. MAGNET WORKING POINT

The machine is operated for high temperature. So it is worthwhile to check out if the magnets are demagnetized or not in eccentric case.
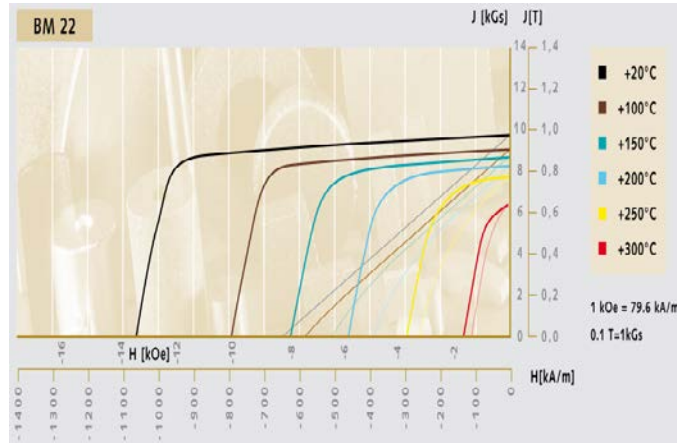

Figure 30: Typical demagnetization curves B(H) and J (H) at different temperatures from Baker Magnetics Company page

Samarium Cobalt (SmCo) magnet has been used in the rotor. And the magnet has bought from a company named Baker magnetics [14]. SmCo has good corrosion resist, high magnetic properties.

The characteristics sheet of BM22 magnet (with B_r = 1T) is given as in Fig 10. In this sheet working point at no load, nominal load and three phase short circuit are investigated. According to specification, maximum temperature winding is 125°C. As per design outside of magnet there is air gap of 2mm which also works as insulation. It can be assumed maximum temperature in magnet up to 150°C is acceptable. calculate the working point of magnet no load condition should be considered at first. Material characteristic sheet demagnetization curve will be used.
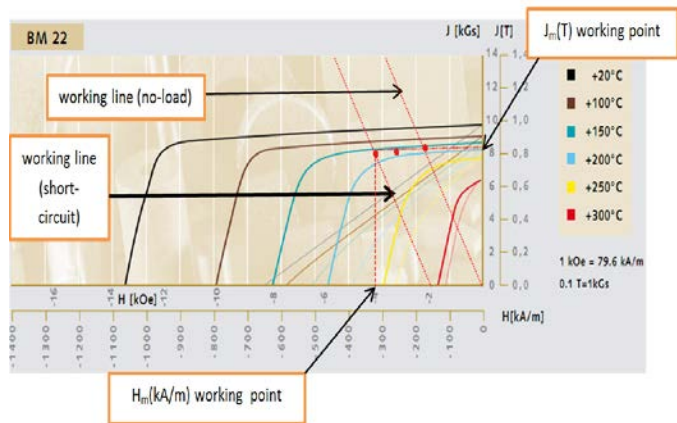

Figure 31: Plotting of working line and working point on Baker magnetics Data Sheet.

For no load condition the mean value of flux density is 0.8T and field intensity is 187.88k A/m. For nominal load condition the mean value of flux density is 0.78T and field intensity is 250.51k A/m. and the values are plotted as in

Fig 31using the methods shown in [15].

The working point can be considered for several temperatures from the intersection of respective B-H curve and working line. Working lines for two different conditions are shown in Fig 31. Working point should be considered for 150°C. As 150°C is assumed earlier as magnet's maximum tolerable temperature.

A. Risk of demagnetization

It is also a significant point to figure out the safe-region of demagnetization. The higher the temperature the lower the periphery of the knee becomes. The higher the temperature the lower the values of remanence flux density will be. At the same time, this high current increase the temperature of magnet and the risk of demagnetization becomes higher.

B. Magnet Point

From the points that are plotted in the graph it can be stated that the magnets are not demagnetized. As it is in safe position inside the knee and far away from the red lines of 300°C.

XI. FLUX WEAKENING

A. Torque-Speed Characteristics

The torque-speed curve can be divided into two regions: constant torque and constant power. At speed lower than the base speed, the rated armature current and the rated excitation-flux Ψ_b are used to produce the rated torque Tb. The supply voltage and output power both increase linearly with speed. This operating range is referred to as the constant-torque region (CTR). At rated speed (1500 rpm), the voltage equals the rated voltage. If speed is desired to increase above base speed, the voltage is kept constant and the flux is decreased. Since torque and speed are inversely proportional, torque decreases with increasing speed. And since the output power is constant beyond the rated speed, this zone is termed as the constant-power region (CPR) or field-weakening region.
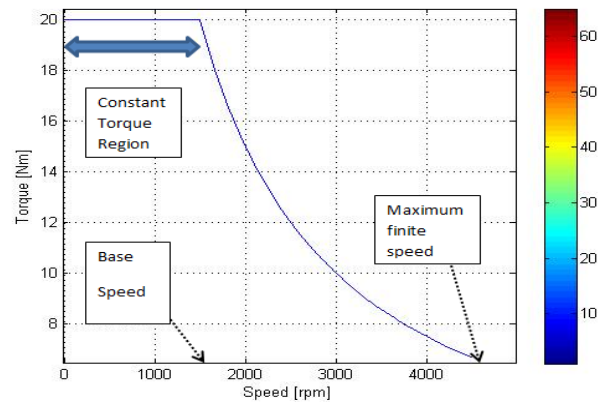

Figure 32: Constant power and torque regions in normalized power vs. speed curve

From Fig 32 the torque vs speed curve is constant upto base speed and it can be reached up to 4500rpm that is shown

in the fig as well. The torque decreases with speed and approaches zero at 4500 rpm (maximum finite speed).
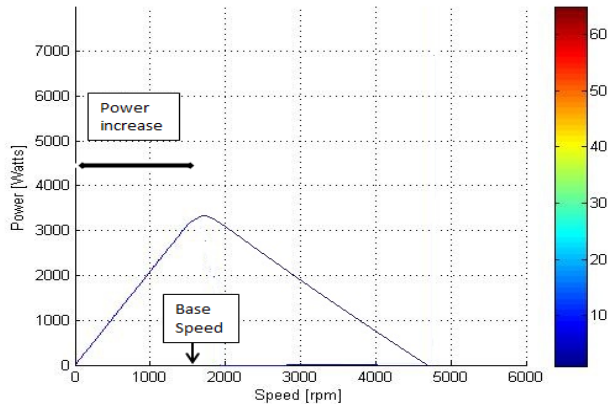
B. Power-Speed Characteristics

Figure 33: power vs. speed curve

The power vs. speed curve of the redesigned machine is shown in Fig33. Here the power increases to its highest peak in base speed. And it touches to x-axis near around 4500 rpm.
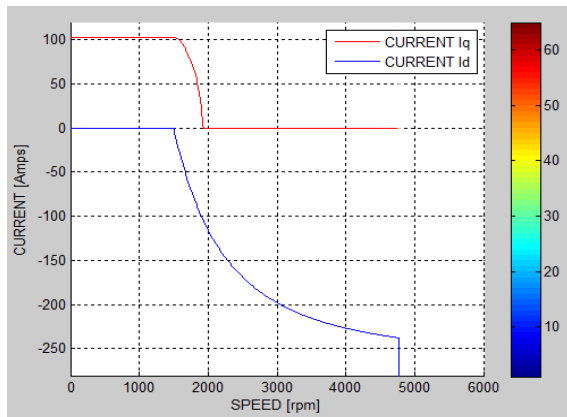
C. Stator Current d-q axis

Figure 34: d- and q-axes current vs. speed

The stator current in dq-axes as a function of the machine speed is shown in Fig 34. It shows the current in d-axis remains zero during constant torque zone (up till 1500 rpm). Once the machine crosses base speed the q-axis current drops and negative current in d-axis rises. This concludes that the stator current vector remains parallel in q-axis until flux-weakening. In the flux weakening zone, flux starts to weaken due to rise in current in negative d-direction which opposes the flux linkage produced by machine's permanent magnet.

It can be seen in Fig 34 that the q-axis current (i_q) remains constant at a value of 100 A (corresponding to a nominal torque of 20 Nm) up to a speed of 1500 rpm, after which it begins to decrease. The d-axis current (i_d), on the other hand, remains equal to 0A in the constant torque region and begins increasing in the negative direction, once the flux weakening region is entered. Hence, it may be said that during the constant torque region, the stator current vector is aligned with the q-axis and has no component in the d-direction.

In the flux weakening region, an increase of d-axis current along the negative d-direction tends to oppose the flux linkage due to the permanent magnet (ψ_m) aligned with the positive d-axis.
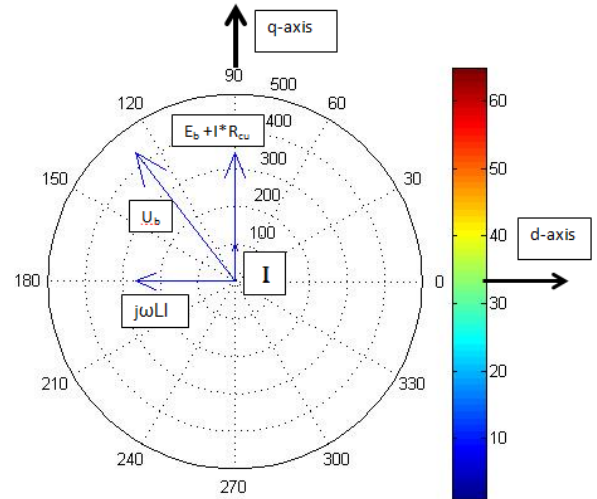

Figure 35: Phase vector diagram at rated operation.

At rated operation, there is no d-axis current. Only q-axis current exists to produce maximum torque. Magnitudes of the vectors is shown in Fig 35 are as eq (1-4) using the data from Smartmotor internal report for badger machine.

$I = 102.93$ A ……………………………………………(eq1)
$E_b + I*R_{cu} = 294 + (102.93*0.5) = 345.465$ V ………… (eq2)
$\omega LI = (2*3.1416*80)*0.0053*102.93 = 274.21$ V……....(eq3)
$U_b = \sqrt{(345.47^2 + 274.21^2)} = 441.1$ V…………….....(eq4)

The magnitude of voltage vector, U_b is always equal to the peak rated phase voltage.

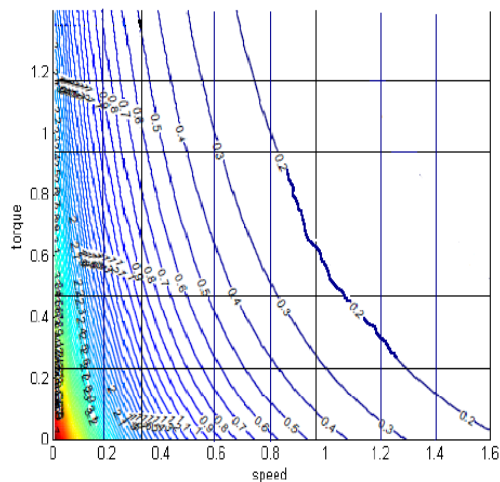## XII. MEASUREMENT/CONTOUR PLOTTING

Figure 36: Contour plotting for the machine

It can be concluded from contour plotting motor efficiency is higher than expected despite that the air-gap is larger than the design value.

The measurements show that the new motor drive is better suited for the load situation. Interestingly the motor efficiency is higher than expected despite that the air-gap is larger than the design value. The flux density was due to the increased air-gap reduced to 0,6 T according to a back-emf measurement. The calculated efficiency is then ~92 %. But the measured efficiency is higher and this may indicate that the rotational losses are smaller than expected.

The more measurements are needed to verify this. The measuring conditions were not the same since the machine runs with variable voltage.

XIII. DESIGN TOOL

A. SmartTool

SmartTool is an analytical Matlab-based software developed by SmartMotor AS. It can calculate a CW-machine based on different geometrical and electrical parameter inputs, such as outer diameter, rated power, rotational speed, voltage level, number of poles and slots, etc. The tool can optimize different machines by varying parameters to achieve high efficiency, low weight, etc.

SmartTool has direct link to Comsol Multiphysics where more accurate calculations can be executed once a machine has been chosen. It makes design and evaluation of machines a rapid process, which allows the designer to optimize different ideas and designs.

B. Comsol Multiphysics

When estimating the performance of a machine, analytical calculations are not accurate enough. Design calculations for coil inductance, air gap flux and magnet leakage, iron losses, back-emf and cogging torque are difficult to evaluate. They should be complimented with Finite Element Analysis (FEA) for better accuracy.

FEA is a numerical technique for solving Partial Differential Equations (PDE) as well as integral equations. The solutions either solve a steady state problem by eliminating the differential equation completely, or reproducing the PDE as an approximating system of Ordinary Differential Equations (ODE). The ODE's are evaluated by numerical techniques such as Euler's method, Simpson, Runge-Kutta, etc.

Comsol Multiphysics is a FEA-simulation software which facilitates all steps in a modeling process. In Comsol, custom definitions of geometry and meshing are possible. Physics can also be specified to fit the purpose. The results can be visualized, with illustrations, graphics and numbers after the multiphysical problem is solved.

Finally 3D design of the badger machine is drawn in Fig 37 using Google sketch up [16]
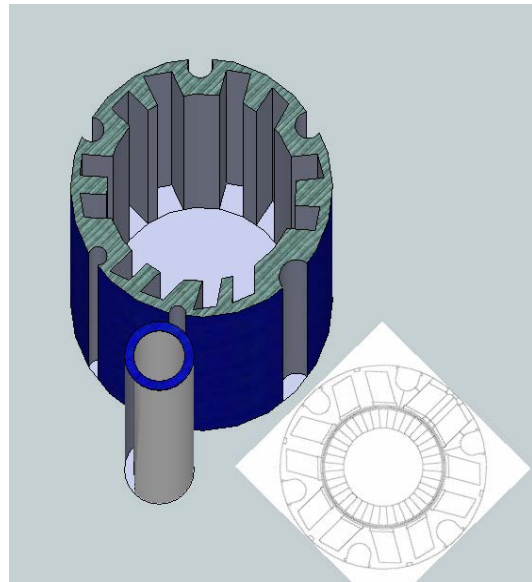

Figure 37: 3D design of badger machine

XIV. 3D OPTIMIZATION- COMSOL AND MATLAB

Many engineers designing rotating electrical machines these days. Currently analytic computer programs are used as the starting point for new designs. Such software solves electromagnetic equations for specific geometries and is typically inexpensive and very quick to run.

Analytic solutions can compromise accuracy and more importantly are "closed" systems that cannot be modified except by the originators. Analytic programs compute an average result for the overall geometry and only approximating.

The alternative can be a CAD tool employing for example, Finite Element Analysis (FEA). These programs typically offer flexible GUI (Graphical User Interfaces)s, allowing users to simulate any design concept with supreme precision and accuracy. Wider analysis options for example, FEA programs can accurately compute eddy currents and naturally evaluate motional effects.

However, the time required for analysis using FEM software in this case, with its three step approach of pre-processing, solving and post-processing is unfavorable. While solution times have steadily decreased over the years owing to steady technological advances in computers, significant effort is still required by the user at the pre-processing stage that is building the geometry and setting the right conditions for solution. Thus, several works have been presented for improving the design environment enhancing the electromagnetic analysis, adapting the dimensional model of the electromagnetic devices and developing an object oriented build up the expected design with sensitivity analysis etc.

The present approach by the author aims to develop a design environment for two and three dimensional analysis of electric motors and generators that could fulfill the needs of both the experienced and less experienced designer. The user

provides the necessary geometric and electrical data for the machine through friendly dialog MATLAB input panel. The code for 3D optimization is attached in Appendix G. The code builds the resulting machine's 3D comparatives analysis in respect to three different parameters. Thusly it performs the necessary solutions and provides simulation results at selected operating conditions. Variations of the given design parameters allows different scenarios to be tested and through an iteration process the user could arrive at a 3D optimized view. Alternatively, the parametric model can be used to drive an optimization tool within the software, setting specific objective functions for the software to achieve. Corresponding data has been taken from COMSOL separately. Yet more works and effort needed to link this code directly to COMSOL.
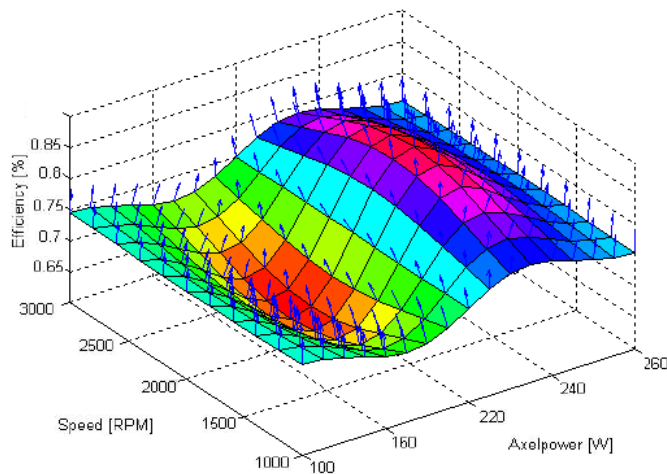
Figure 38: 3D optimized figure for land plot of efficiency

Fig 38 shows the efficiency of previous machine based on measurements made in the laboratory. the plot is generated using the interpolation done in Matlab. The figure comes out two distinct areas with high efficiency, where the first starts at rated power and follows the line for rated speed (1500 rpm). Then the second starts at 220 watts and rises along the line of 2500 rpm. Since this area has the greatest extent in power with high efficiency (80%) it is natural to assume this rotational speed by the choice of conditions for the exchange. In this way the efficiency of engine with the engine operation is optimized at a constant speed and variable load control signal. Simulations showed that for a system efficiency of over 70% (assuming constant efficiency at 50%), the optimum speed to be more than 3000 rpm.

By following the 3D area and basing the calculation of 1500 rpm the idea gives a better efficiency at loads above 150 watts. In order to take advantage of this exchange should the strategy involve a driving pattern with accelerations. So not constant speed throughout the race.

We have the following conclusions and explanations for the analytical results from Fig 38:

The machines have high efficiencies (more than 90%), which increases along with an increase of axel power to the maximum value of around 92% for ten pole machines and then decreases. On the same note by increasing the axel power it is also possible to increase the machine torque and the stator copper loss should decreases due to reduced end-winding length, which implies increased machine efficiency. On the other hand, both eddy-current and hysteresis losses increase because the operating frequency increases proportionally to the number of poles in order to achieve the desired speed. This will decrease the machine efficiency on the contrary.
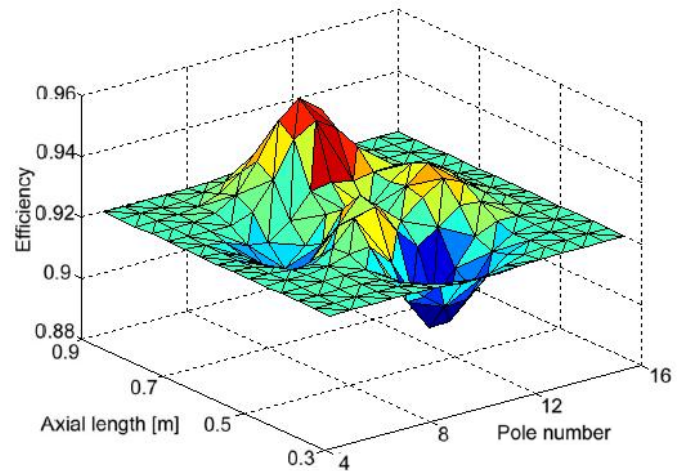

Figure 39: 3D optimized figure for land plot of efficiency

For further optimization as three parameters: Efficiency, Axial length and pole number has been chosen as like Fig 39. Assume the investigated machines have a high power factor. And the pole number will mostly varied from 8 to 12. The reason is that for low-pole-number machines, the active winding length increases rapidly with an increase of the pole number so that the back EMF has a chance increases even if the leakage flux increases in the air gap. And in case of high pole-number machines, the fringing factor becomes dominant.

XV. OPTIMIZATION IMPLEMENTATION AND SIMULATION

A. *Optimization Matlab Tool*

The optimtool is a new add-on 'toolbox' available in Matlab 2011a with the established commercial packages. A FEA model for a generator or motor can be optimized using templates by optimizing few parameters of machine. Tool has been designed for most common electrical machine types. As with analytic computer programs, the template represents the most characteristic comparative result of the calculative parameters. One important feature of the tool is that templates are built using generic scripting and the underlying code can easily be modified by users, providing the freedom to optimize and analyze customized outputs, including special proprietary features.

The optimization toolbox includes a graphical user interface (GUI) that is easy to use. To activate one need to simply type *optimtool* at the command line.

B. *Function handle:*

a MATLAB value that provides a means of calling a function indirectly.

Function handles can be passed in calls to other functions
Function handles can be stored in data structures for later use
The optimization and genetic algorithm toolboxes make extensive use of function handles

Process of function handle:

For the functions handling following steps has been followed:

1. To create a function that takes in two scalar-valued arguments and outputs both the function and gradient

2 To create a handle for this function and use *ezsurf* to plot the function

3 To create an optimization-ready handle for this function and solve using different starting points using:

-fminunc, medium scale, derivatives approximated by solver
-fminunc, medium scale, gradient supplied
-fminsearch,ga etc.

4 To compare the algorithms on the following measures:

a. *Robustness*: ability to _nd a global optimum and dependence of performance on initial guess

b. *Efficiency*: how many function evaluations were required

Supplying Gradients:

-It may be desirable to analytically specify the gradient of the Function. To do this, the named function must return two outputs: *the function value* and the *gradient*

-For the optimization toolbox, only one vector-valued input argument should be used
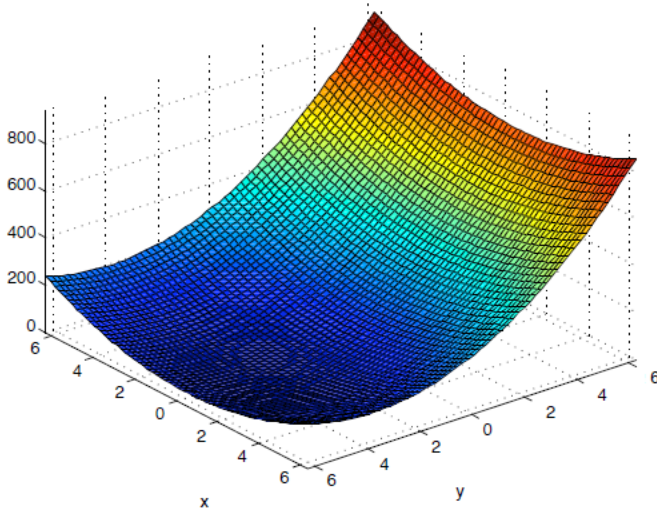
Figure 40: 3D optimized surface plot

With GUI, the author would like to 'track' the progress of the optimizer

-Under options, set Level of display: iterative

-Under plot functions, check: function value

-When ga is used, it is needed to check 'Best fitness' and 'Expectation' to track the fittness of the best member of the population and the average fitness.

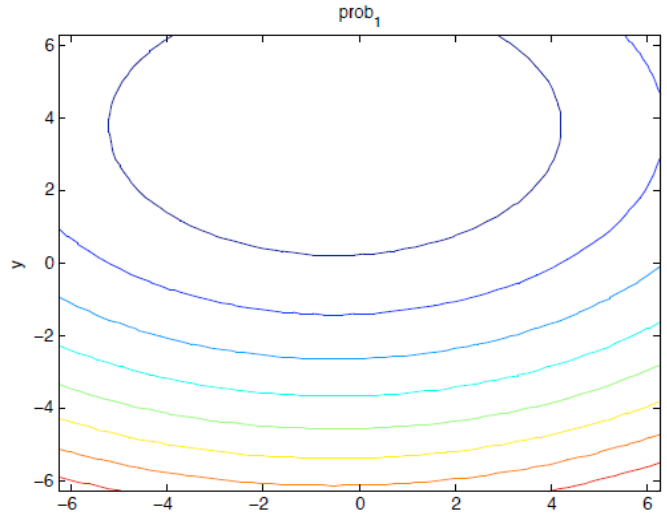3D optimized function value for surface and contour plot is drawn thereby with optimtool in Fig 40 and Fig 41.

Figure 41: 3D optimized contour plot

XVI. CONCLUSION AND DISCUSSION

State of the art has been found with Smartmotor AS machine position that will be helpful for presenting its performances to customers. From the figure it is visualized Badger machine and state-of-art of machine follows equal performance. This is considered in terms of torque and power.

The dimensional aspects determining the cogging torque of the machine are also investigated. It was eccentric and also had arbitrary misplacement of magnets. And the mechanical tolerance along with Cogging torque in every third position of the rotor with detailed experiment description has been mentioned.

Later, finite element analysis is used to quantify the cogging torque in design process. During COMSOL simulation in every condition there was an impact of 6th harmonics is noticed while investigating cogging torque of machine. In new design the amplitude of 6th harmonic also has been reduced. Cogging torque as a function of rotor angle at different skewing angle has been investigated with this paper as a possible solution of cogging torque.

From the flux weakening calculation it is observed the speed can be incrased upto 3 times to its rated speed. And different calculation with a phasor diagram is plotted in Fig 32-34.

The complexity of using different versions of COMSOL has also an affect on the results. It can be concluded more time, skill and experience is needed for more accurate result and outputs for a perfect accomplishment of the project.

Magnet skewing with different shape investigated in details. Though the investigation is theoretical any of the shape can be implemented for real rotor in order to reduce cogging torque.

Mmf distribution and winding, distribution functions of machine also analyzed for better understanding. During no load test the impact on magnet working point and flux weakening are shown.

Finally a short investigation on overall electrical machine optimization technique analyzed in brief also new Matlab code has been written by author which can be a powerful tool for a machine designer in future.

XVII. SUGGESTED FUTURE WORK

This paper presents an overview of minimizing cogging torque of an electrical downhole machine. Yet many works can be accomplished with this project in future. The new 10 magnet design is proposed with this paper. As per expectation it should be cost effective comparing the design of Hallbach Array Rotor when magnet area is reduced in new design. It is thereby suggested to investigate the cost of two rotors. And skewing effect can also minimize the cogging torque of machine which can further be investigated and implemented. With improvement of optimization tool a two and three-dimensional FEA model for a generator and motor can be created in minutes.

The machine should be tested with a frequency converter and a positional encoder. This would give the opportunity to run a pure q-axis current, giving a much better platform for an evaluation of the machine performance, both in terms of torque density and in examining the saturation issues present in the machine. A frequency converter would of course give the opportunity to run the machine as a motor as well as a generator.

The machine still has room for improvement by reducing the motor weight with the use of Halbach arrays, reducing the eddy-current losses. Also the air-gap could be further reduced to increase efficiency. Other observations and experiences during the no load test are also discussed in this paper for improvements on the electromagnetic design of the machine. It is recommended to work further on magnet skewing with hallbach array design.

Further work should also be put into the examination of losses and resistances, with more detailed measurements of the torque in order to get better values of the machine input power and the losses as well. The rotor eccentricity show little effect on the phase voltages, but some work should still be put into the examination of possible power fluctuation caused by this. Still another task that can be performed are the testing of alternative rotors, such as skewing the rotors already made and testing of a more optimized 10pole rotor. To build up a new rotor it will take around 20kNOK and the new design happens to be best suitable design for this

REFERENCES

[1] SMARTTOOL, A MATLAB based permanent magnet synchronous machine design tool developed by SMARTMOTOR AS.

[2] http://en.wikipedia.org/wiki/Cogging_torque#Reducing_cogging_torque

[3] M. S. Islam, S. Mir and T. Sebastian, "Issues in reducing the cogging torque of mass-produced permanent magnet brushless dc motor," IEEE Trans. on Industry Applications, vol. 40, no. 3, pp.813-820, May/June 2004.

[4] D.C. Hanselmann, Dr., " Brushless Permanent-Magnet Motor Design" First ed. New york: McGraw-Hill, Inc,.1994.

[5] N. Bianchi and S. Bolognani, "Design techniques for reducing the cogging torque in surface-mounted PM motors," IEEE Trans. On Industry Applications, vol. 38, no. 5, pp. 1259-1265, September/ October 2002.

[6] T. Li and G. Slemon, "Reduction of cogging torque in permanent magnet motors," IEEE Trans. on Magnetics, vol. 24, no. 6, pp. 2901-2903, November 1988.

[7] T. Ishikawa and G. Slemon, "A method of reducing ripple torque in permanent magnet motors without skewing," IEEE Trans. on Magnetics, vol. 29, no. 2, pp. 2028-2031, March 1993.

[8] Z. Q. Zhu and D. Howe, "Effect of slot and pole number combination on cogging torque in permanent magnet machines," Unknown.

[9] E. Favre, L. Cardoletti and M. Jufer, "Permanent-magnet synchronous motors: A comprehensive approach to cogging torque suppression," IEEE Trans. on Industry Applications, vol. 29, no. 6, pp. 1141-1149, November/December 1993.

[10] M. S. Islam, S. Mir and T. Sebastian, "Issues in reducing the cogging torque of mass-produced permanent magnet brushless dc motor," IEEE Trans. on Industry Applications, vol. 40, no. 3, pp.813-820, May/June 2004.

[11] Z.Q. Zhu and D. Howe, "Analytical Prediction ofCogging Torque in Radial Field Permanent Magnet Brushless Motors," IEEE Transactions on Magnetics,Vol. 28, No. 2., 1992, pp. 1371-1374

[12] COMSOL multiphysics http://www.comsol.se

[13] F. Meier and J. Soulard, "Emetor- An educational web-based design tool for permanent magnet synchronous machine," Proceedings of the International Conference on Electrical Machine,2008 Paper ID 866.

[14] http://www.bakkermagnetics.com/images/0236880001227637312.pdf

[15] S. Ruohu, 'Demagnetization of Permanent Magnets in electrical mahcines' Helsinki university of Technology, 2006

[16] http://sketchup.google.com/

[17] Internal report provided by Smartmotor AS.

[18] T.J.E. Miller, "Brushless Permanent-Magnet and Reluctance Motor Drives," Oxford University Press, New York, 1989.

[19] R.P. Deodhar, D.A. Staton, T.M. Jahns, T.J.E. Miller, "Prediction of Cogging Torque Using the Flux-MMF Diagram Technique," IEEE Transactions on Industry Applications, Vol. 32, No. 3, May/June 1996, pp. 569-576.

[20] http://www.mathworks.se/products/datasheets/pdf/optimization-toolbox.pdf

[21] C. C. Hwang, S. P. Cheng, and P. L. Li, "Design optimization for cogging torque minimization and efficiency maximization of an SPM motor, "IEEE IEMDC Conference proceedings, vol. 1, pp. 642-646, May 2007.

[22] D. J. Shin and B. Kwon, "Multi-objective optimal design for inwheel permanent magnet synchronous motor, "International conference on electrical machines and systems, pp. 1-5, November 2009.

[23] S. X. Chen, T. S. Low and B. Bruhl, "The robust design approach for reducing cogging torque in permanent magnet motors for CDROM spindles, "IEEE Trans. on Magnetics, vol. 34, no. 4, pp. 2135-2137, July 1998.

[24] C. C. Hwang and T. Y. Lin, "Design optimization for cogging torque minimization of a high-speed 2-pole IPM machine, "IEEE Conf. on Electromagnetic field computation, pp. 237-237, June2006.

[25] G. Taguchi, S. Chowdhury and Y. Wu, "Taguchis's quality engineering handbook", John Wiley publication 2004.

[26] http://www.ca-bd.org

BIOGRAPHY

Aasim Ullah was born in Doha, Qatar. He received the Bachelors of Engineering degree in Electrical Engineering in 2009 from **Ahsanullah Uni of Science & Tech, Bangladesh** and currently a Master student at the Department of Electric Power Engineering, **Norwegian University of Technology and Science (NTNU),** Trondheim, **Norway**. He also studied at **Royal Institute Technology** in Stockholm, **Sweden** as an exchange student. He wrote his Master's thesis in cooperation with **SmartMotor AS**. His current research interests are in electrical machine design, electromagnetic, power electronics and drives.

APPENDIX A-COMPANY DATA
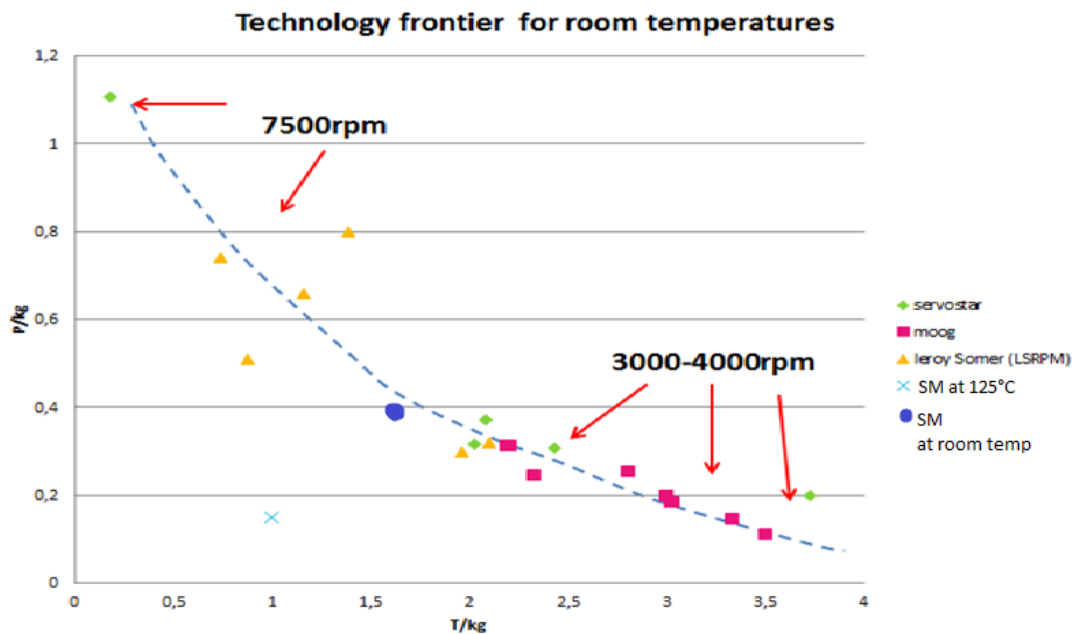
Fig A1: Technology frontier from room temperature

	Motor designation	P (kW)	T (Nm)	m (kg)	P/m (kW/kg)	T/m (Nm/kg)	Rated temp	Volume (m3)	Volume (l)	P/V (kW/m3)	T/V (Nm/m3)	P/V (kW/l)	T/V (Nm/l)
	BH-624G	4,6	86,2	23,1	0,199	3,73	45°C	0,005	4,87	944,56	17700,2	0,94456	17,7
	BH-624E	7,3	46,9	23,1	0,316	2,03	45°C	0,005	4,88	1495,9	9610,66	1,4959	9,611
Kollmorgen/ Servostar	BH-624C	7,1	56,2	23,1	0,307	2,432	45°C	0,005	4,88	1454,9	11516,4	1,45492	11,52
	BH-426C	5,9	33,2	15,9	0,371	2,08	45°C	0,004	3,53	1671,4	9405,1	1,67139	9,405
	MH-226E	1,7	10,5	9,5	1,105	0,178	45°C	0,002	1,58	1075,9	6645,57	1,07595	6,646
	BN 34-25AF	0,328	0,4237	1,05	0,312	2,192	25°C	3E-04	0,339	967,55	1249,85	0,96755	1,25
	BN 34-45AF	0,459	1,3276	2,499	0,184	3,024	25°C	6E-04	0,611	751,23	2172,83	0,75123	2,173
	BN 34-35EU	0,446	0,827	1,758	0,254	2,804	25°C	5E-04	0,52	857,69	1590,38	0,85769	1,59
Moog	BN 34-45EU	0,459	1,33	2,495	0,184	3,03	25°C	7E-04	0,669	686,1	1988,04	0,6861	1,988
	BN 42-23EU	0,456	0,721	1,843	0,247	2,33	25°C	5E-04	0,516	883,72	1397,29	0,88372	1,397
	BN 42-33EU	0,584	1,51	2,949	0,198	3	25°C	7E-04	0,74	789,19	2040,54	0,78919	2,041
	BN 42-43EU	0,598	2,41	4,054	0,148	3,33	25°C	1E-03	0,96	622,92	2510,42	0,62292	2,51
	BN 42-53EU	0,58	3,19	5,16	0,112	3,5	25°C	0,001	1,18	491,53	2703,39	0,49153	2,703
	LSRPM90L	8,6	15	17	0,51	0,88	40°C	0,008	7,84	1096,9	1913,27	1,09694	1,913
	LSRPM200L	70	122	135	0,66	1,16	40°C	0,095	95	736,84	1284,21	0,73684	1,284
Leroy Somer	LSRPM200L1	140	243	175	0,8	1,39	40°C	0,095	95	1473,7	2557,89	1,47368	2,558
	LSRPM280SC	105	668	330	0,318	2,1	40°C	0,21	210	500	3180,95	0,5	3,181
	LSRPM315MR	220	1401	715	0,3	1,96	40°C	0,346	346	635,84	4049,13	0,63584	4,049

Table A: Company data and detailed calculation found from Company catalogues

APPENDIX B-COMSOL SIMULATION (ECCENTRIC CONDITION, HALLBACH ARRAY DESIGNED ROTOR)
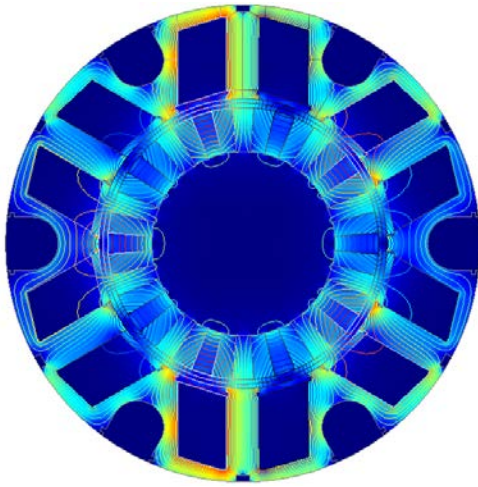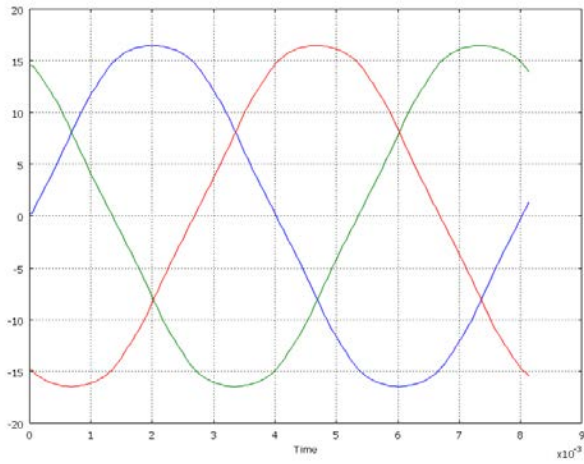

Fig B1: COMSOL simulation picture of full periphery
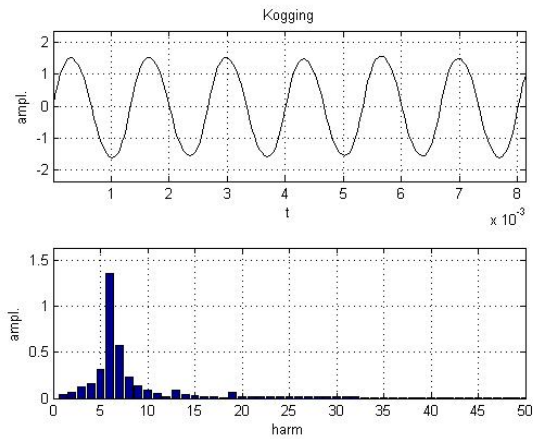

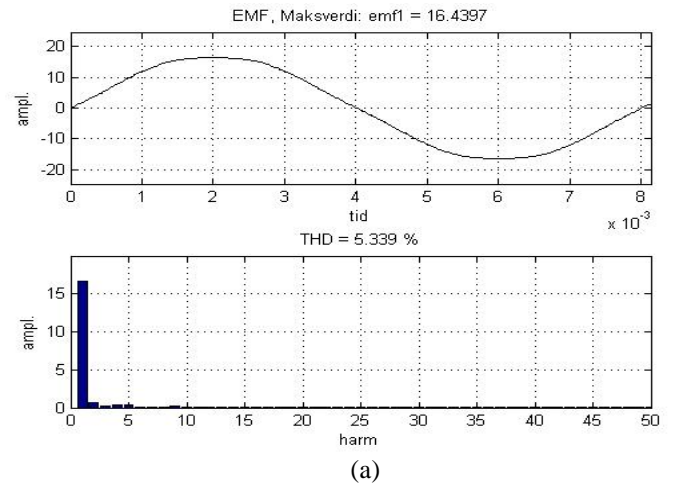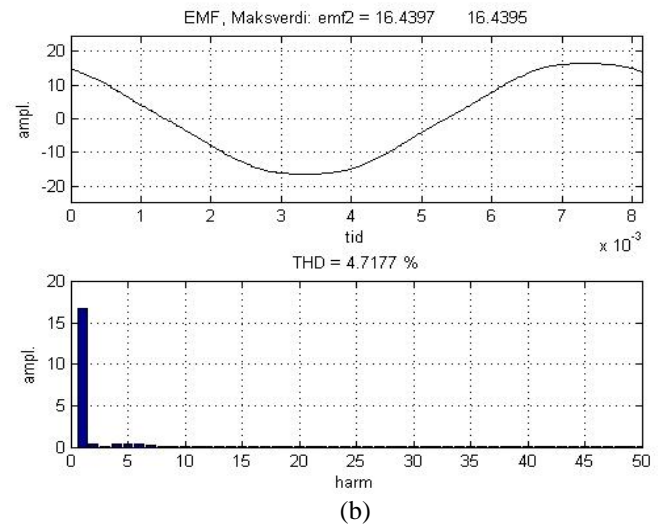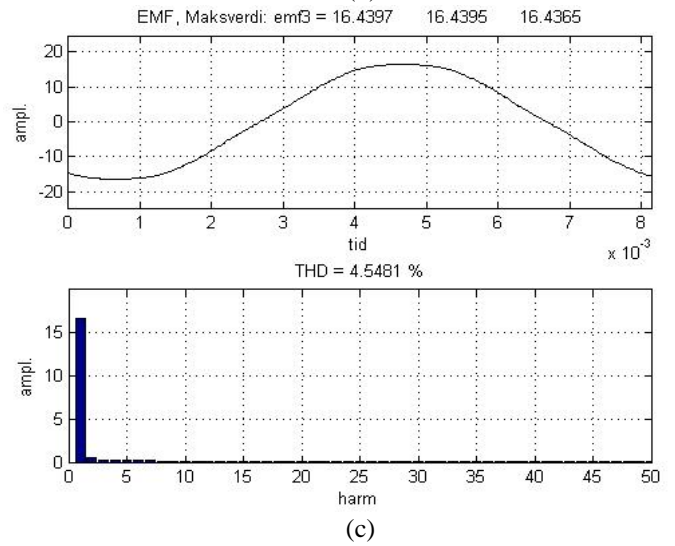Fig B2: 3EMF voltage of machine

Fig B3: Cogging Torque with 6th harmonic distortion

(a)

(b)

(c)

Fig B4: 3EMF voltage of machine

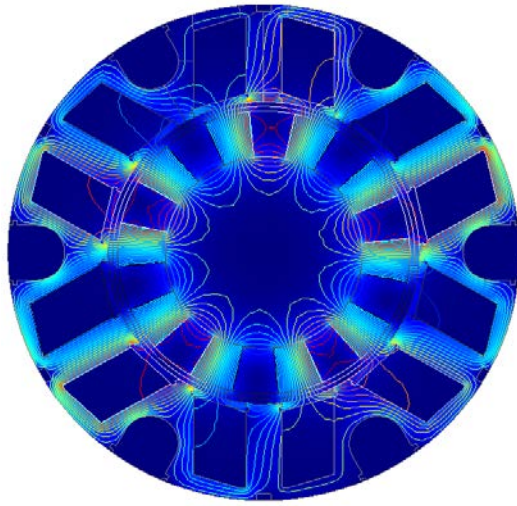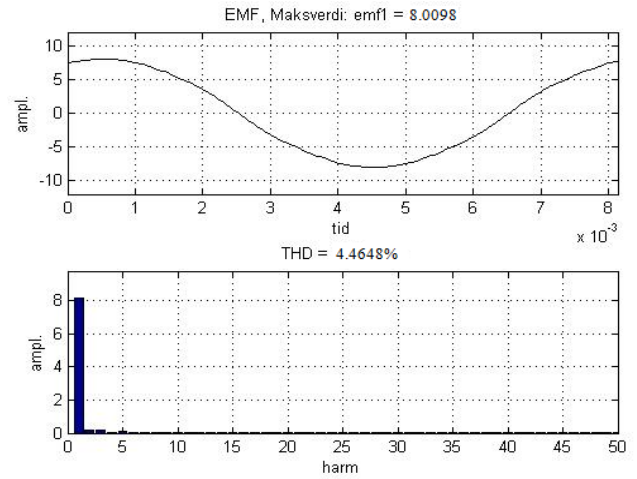APPENDIX C- COMSOL SIMULATION WITH 10 MAGNETS (ECCENTRIC CONDITION, MAGNET 50%-EPOXY50%)

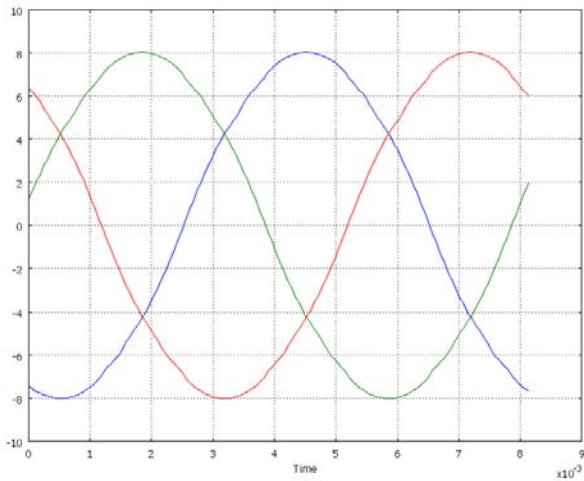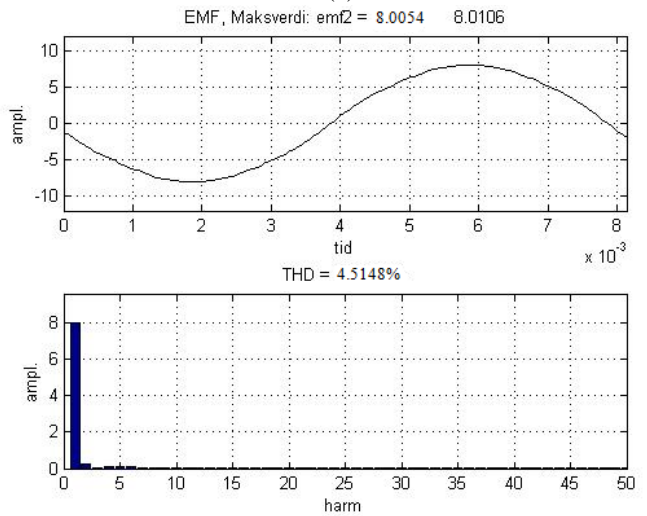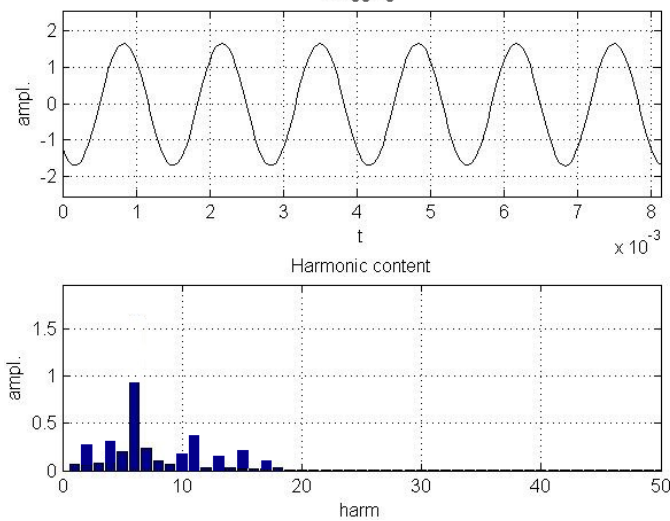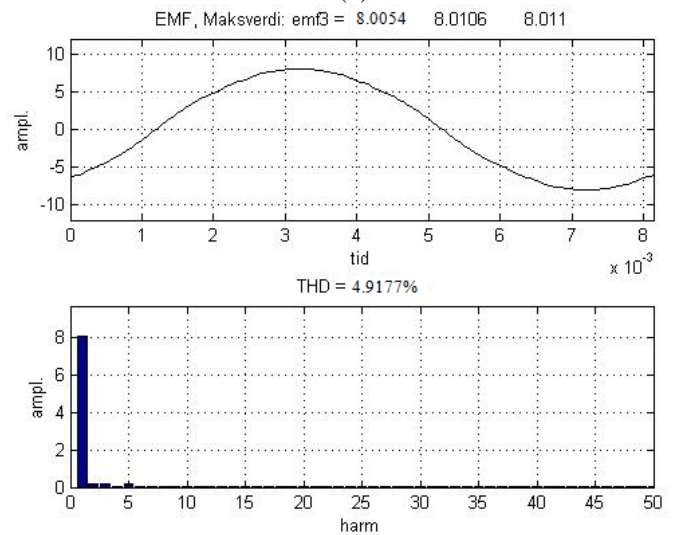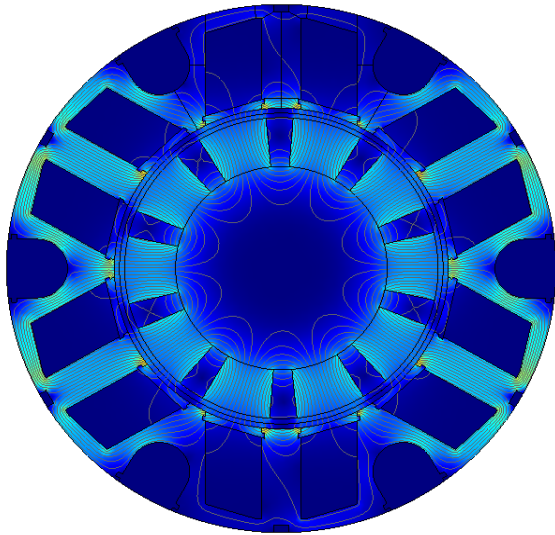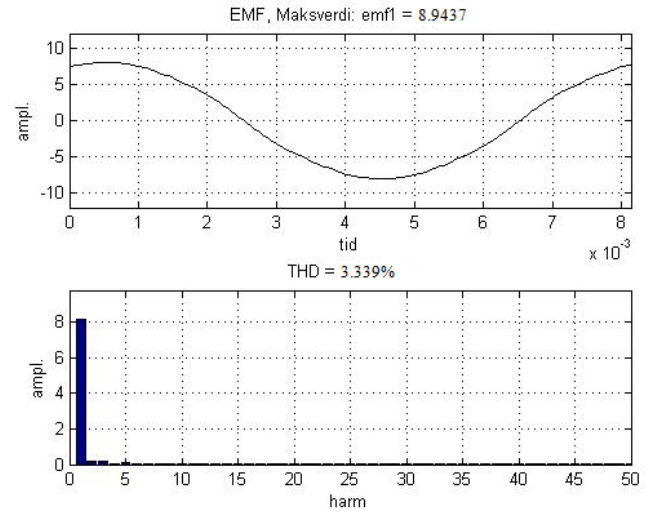Fig C1 : COMSOL simulation picture of 10 magnets machine

Fig C2 : 3 EMF voltage of 10 magnets machine

Fig C3: Cogging Torque with 6th harmonic distortion

(a)

(b)

(c)

Fig C4 : 3EMF voltage of 10 magnets machine

APPENDIX D- COMSOL SIMULATION WITH 10 MAGNETS (ECCENTRIC CONDITION, MAGNET75%-EPOXY 25%)
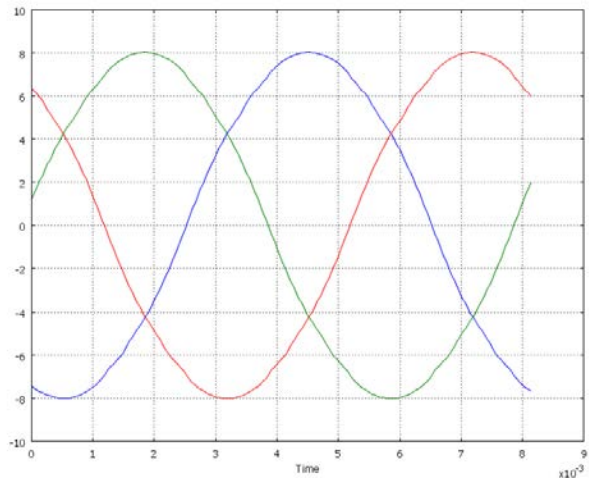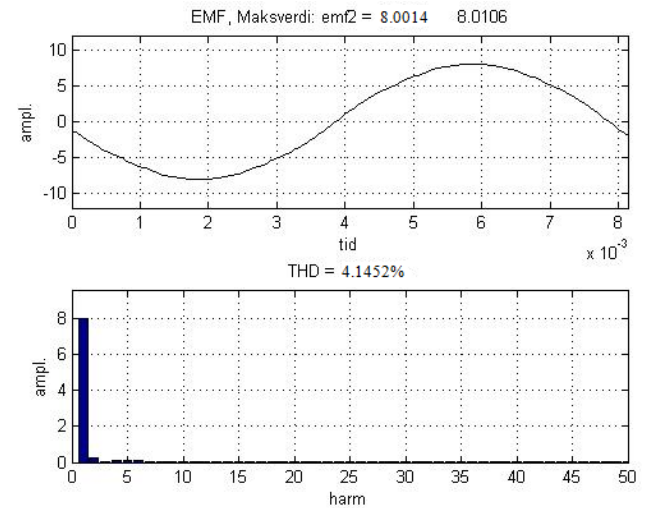

Fig D1: COMSOL simulation picture of full periphery

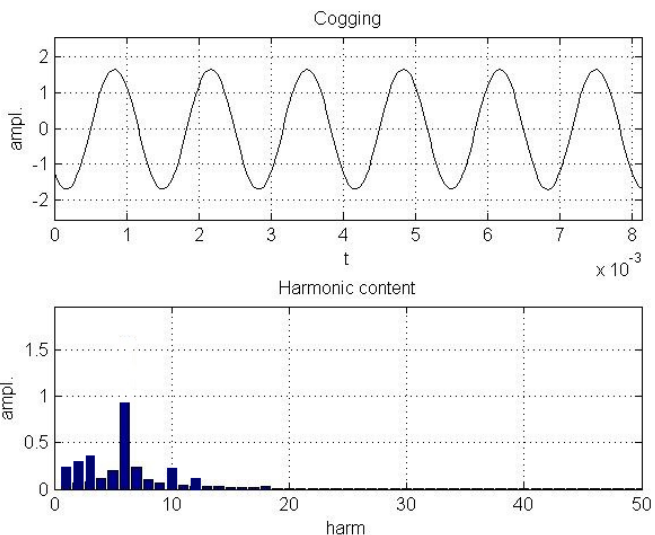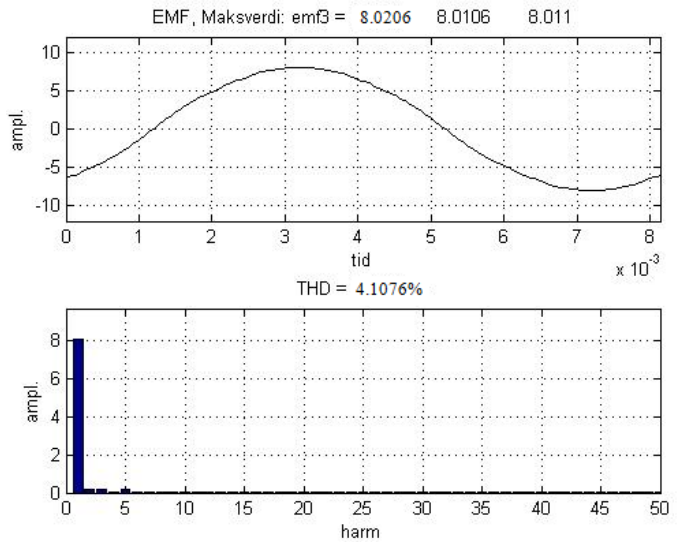Fig D2: 3EMF voltage of machine

Fig D3: Cogging Torque with 6th harmonic distortion

(a)

(b)

(c)

Fig D4: 3EMF voltage of machine

APPENDIX E- COMSOL SIMULATION WITH 10 MAGNETS (ECCENTRIC CONDITION, MAGNET 90%-EPOXY 10%)
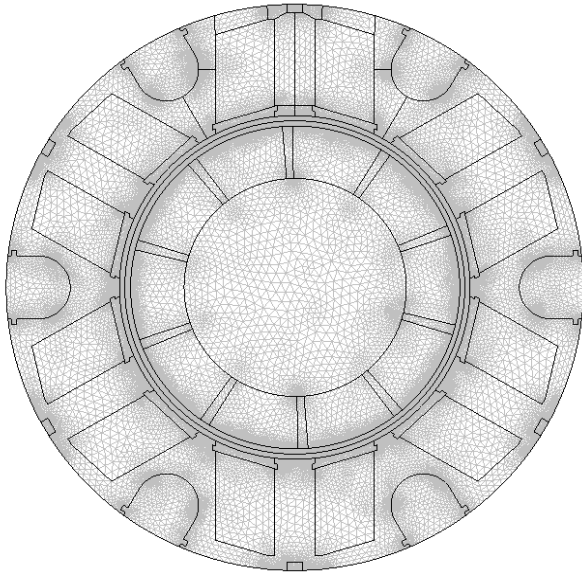

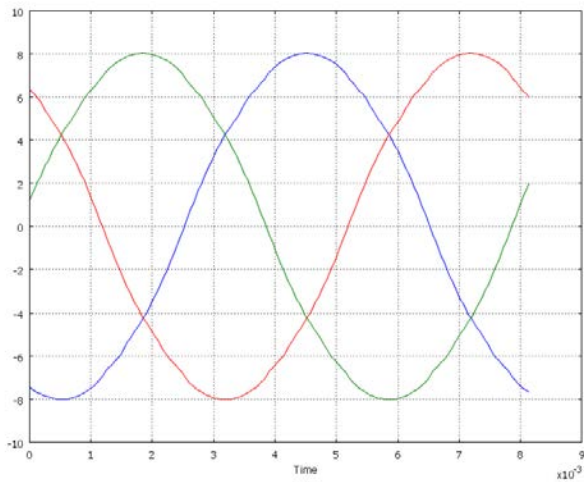Fig E1: COMSOL simulation picture of full periphery
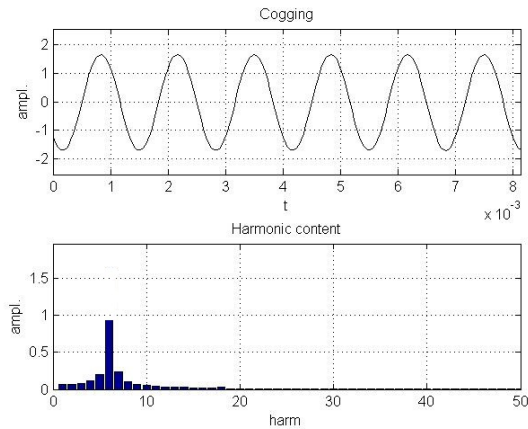

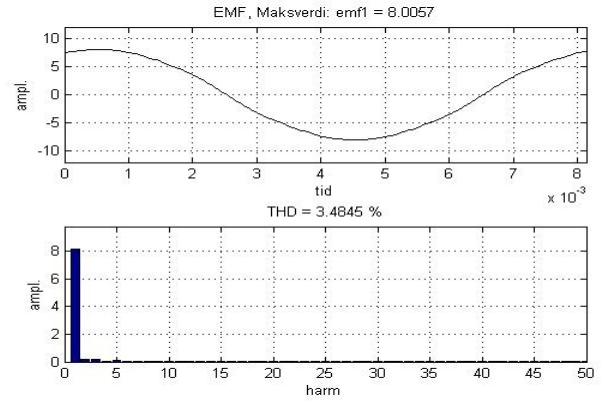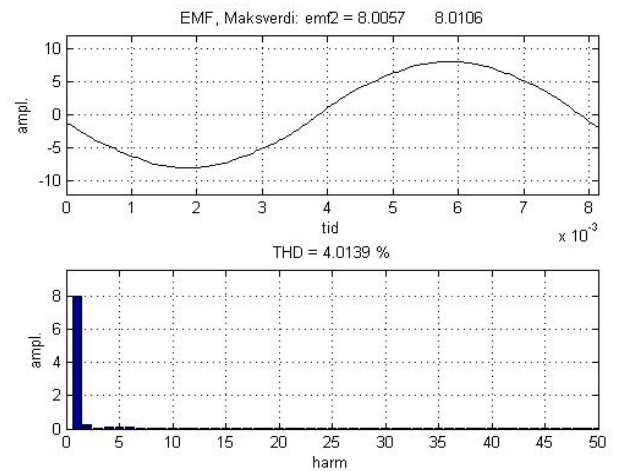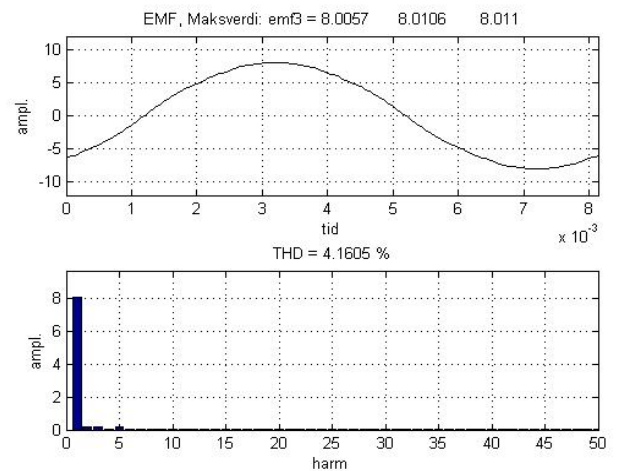Fig E2: 3EMF voltage of machine

Fig E3: Cogging Torque with 6ᵗʰ harmonic distortion

(a)

(b)

(c)

Fig E4: 3EMF voltage of machine

APPENDIX F-MATLAB

```matlab
% Flux weakening for Badger Machine
%Code by Aasim Ullah
%using the badger-machine data from internal report of Smartmotor AS
clear;
close all;
clc
p=10;        % no of poles
Eb=294; %Peak phase induced voltage
Ub=300; %Peak value of phase voltage.


nB = 1500; % base speed in rpm


wb_mech = nB/60*2*pi;   %Max mechanical speed of the constant torque region.
wb = wb_mech*p/2; %rated electrical frequency.


Tb = 20; % base torque: rated torque in Nm.
I = 102.93; % Peak phase current.
L = 5.3e-3; % Inductance in H.


Rcu= 0.5; % Phase resistance in ohms.


psi_M = Eb/wb; % Flux linkage due to permanent magnets
psi_B = Ub/wb; % Base flux linkage
psi_N = psi_M/psi_B  % Nominal flux linkage



In = 1/psi_N;
IB = I/In;
LN = psi_N*sqrt(1-psi_N^2) %Nominal inductance in p.u
LB = L/LN  %base inductance
LB = (3*p*Ub^2)/(4*Tb*wb^2)


L = LN*LB


%n_max = 1/(psi_N-sqrt(1-psi_N^2))*nB
Trated= 20; % Rated Torque

% CONSTANT TORQUE REGION
w_constantT = [0:1:wb_mech];   %A row vector
T_constantT = psi_N * In * Trated .* ones(size(w_constantT)); %Torque calculation for
the constant torque region.

% PLOTTING OF PHASE VECTOR DIAGRAM FOR RATED CONDITIONS
current=j*I;
emf=j*Eb;
resistive_drop=j*(I*Rcu);
L_em=3.296*10^-3;
ind_vol_drop=-wb*L_eme*I;
phase_vol=emf+resistive_drop+ind_vol_drop;
Z=[current;emf + resistive_drop;ind_vol_drop;phase_vol];
compass (Z)

% CONSTANT POWER REGION UP TILL MODE 2.
w_constantP = [1:0.01:3.18495]; % 3.18495 is the normalized speed at which mode3
operation begins.
%w_constantP = [1:0.01:n_max/nB];
gama = asin(((w_constantP.*psi_N).^2+(w_constantP.*(LN/psi_N)).^2-
1)./(2.*w_constantP.^2.*LN));
```

```matlab
Iq = In.*cos(gama);
Id = -In.*sin(gama);
T_constantP = psi_N*Trated.*Iq;
w_constantP = w_constantP.*(2*pi*nB/60);
Tk=(Tb*nB)./((w_constantP./(2*pi)).*60); % Ideal torque characterictic for the
constant power region up till mode 2.

% CONSTANT POWER REGION FOR MODE 3.
w_constantP3 = [3.18495:0.01:7]; % 3.18495 is the normalized speed at which mode3
operation begins.

gama = atan(-(w_constantP3.*psi_N)); %Optimized angle for mode 3 operation.
Id3= -(psi_N/LN);    %d-axis current component which remains constant during mode3
operation.
I3 =  Id3./sin(gama); %Calculation of the current vector during mode3 operation.
Iq3 = I3.*cos(gama); %q-axis current component during mode3 operation.
T_constantP3 = psi_N*Trated.*Iq3; %Calculation of torque during mode3 operation.
w_constantP3 = w_constantP3.*(2*pi*nB/60);
Tk3=(Tb*nB)./((w_constantP3./(2*pi)).*60); % Ideal torque characterictic for the
constant power region up till mode 2.

% COMBINING THE THREE REGIONS
T = [T_constantT T_constantP T_constantP3]; % Combining torque for the two regions.
%T = [T_constantT T_constantP];
t = [T_constantT Tk Tk3];            % Combining ideal torque for the two regions.
%t = [T_constantT Tk ];
w = [w_constantT w_constantP w_constantP3];
%w = [w_constantT w_constantP];
I_Q = IB.*[In.* ones(size(w_constantT)) Iq Iq3]; %q-axis current over the entire range
.i.e the constant torque region and the field weakening region.
%I_Q = IB.*[In.* ones(size(w_constantT)) Iq];
I_D = IB.*[zeros(size(w_constantT)) Id Id3.*ones(size(w_constantP3))]; %d-axis current
over the entire range .i.e the constant torque region and the field weakening region.
%I_D = IB.*[zeros(size(w_constantT)) Id];
% OUTPUT POWER.
P = w.*T;

% PLOTTING OF TORQUE-SPEED and POWER-SPEED CURVES.

figure;
hold on
plot(60/(2*pi)*w,T,'r') % speed in rpm versus torque in Nm.
plot(60/(2*pi)*w,t,'b')% speed in rpm versus T=k/w.
Legend('Torque','Torque=k/w');
grid on
xlabel ('Speed [rpm]')
ylabel ('Torque [Nm]')
figure;
hold on
plot(60/(2*pi)*w,P) % power in watts versus speed in rpm
grid on
xlabel ('Speed [rpm]')
ylabel ('Power [Watts]')

% PLOTTING OF d-axis and q-axis CURRENTS versus motor speed.

figure;
hold on
plot(60/(2*pi)*w,I_Q,'r')
plot(60/(2*pi)*w,I_D,'b')
grid on
xlabel ('SPEED [rpm]')
```

```matlab
ylabel ('CURRENT [Amps]')
legend ('CURRENT Iq','CURRENT Id')


Ind;

n_max = (Ub./(Eb-(wb.*I).*L)).*nB

figure
hold on
plot (I,n_max)
grid on
xlabel ('CURRENT [Amps] ')
ylabel ('MAXIMUM SPEED [rpm]')

%Re-estimation of CPSR of motor
n_max=11313;
psi_N=0.77028;
In=1/psi_N;
I=102.93;
IB=I/In;
LN = psi_N*sqrt(1-psi_N^2);

%CONSTANT TORQUE REGION
w_constantT = [0:1:wb_mech];   %A row vector
T_constantT = psi_N * In * Trated .* ones(size(w_constantT));

%CONSTANT POWER REGION
w_constantP = [1:0.01:n_max/nB];

gama = asin(((w_constantP.*psi_N).^2+(w_constantP.*(LN/psi_N)).^2-
1)./(2.*w_constantP.^2.*LN));

Iq = In.*cos(gama);
Id = -In.*sin(gama);
T_constantP = psi_N*Trated.*Iq;
w_constantP = w_constantP.*(2*pi*nB/60);
Tk=(Tb*nB)./((w_constantP./(2*pi)).*60);

%COMBINING THE TWO REGIONS
T = [T_constantT T_constantP];
t = [T_constantT Tk];
w = [w_constantT w_constantP];
I_Q = IB.*[In.* ones(size(w_constantT)) Iq]; %q-axis current over the entire range
.i.e the constant torque region and the field weakening region.
I_D = IB.*[zeros(size(w_constantT)) Id]; %d-axis current over the entire range .i.e
the constant torque region and the field weakening region.

%OUTPUT POWER.
 P = w.*T;

%PLOTTING OF TORQUE-SPEED and POWER-SPEED CURVES.

figure;
hold on
plot(60/(2*pi)*w,T,'r') % speed in rpm versus torque in Nm.
plot(60/(2*pi)*w,t,'b')% speed in rpm versus T=k/w.
grid on
xlabel ('Speed [rpm]')
ylabel ('Torque [Nm]')
Legend('Torque','Torque=k/w');
figure;
```

```
hold on
plot(60/(2*pi)*w,P) % power in watts versus speed in rpm
grid on
xlabel ('Speed [rpm]')
ylabel ('Power [Watts]')

% PLOTTING OF d-axis and q-axis CURRENTS versus motor speed.

figure;
hold on
plot(60/(2*pi)*w,I_Q,'r')
plot(60/(2*pi)*w,I_D,'b')
grid on
xlabel ('SPEED [rpm]')
ylabel ('CURRENT [Amps]')
legend ('CURRENT Iq','CURRENT Id')
```

APPENDIX F- MATLAB 3D OPTIMIZATION

```
figure
[X,Y] = meshgrid(-2:0.25:2,-1:0.2:1);
Z = X.* exp(-X.^2 - Y.^2);
[U,V,W] = surfnorm(X,Y,Z);
quiver3(X,Y,Z,U,V,W,0.5);
hold on
surf(X,Y,Z);
colormap hsv
view(-35,45)
axis ([-2 2 -1 1 -.6 .6])
hold off
```